

Gamma-Ray Bursts at High Redshift

Matthijs Dries

supervisor: Prof. Dr. Marco Spaans
Kapteyn Astronomical Institute, Groningen

March 11, 2008

Abstract

Gamma-Ray Bursts (GRBs) are very energetic explosions. Probably they are the most energetic events in our universe following the Big Bang. A GRB is characterized by an intense flash of γ -radiation, in which $\sim 10^{51} - 10^{53}$ ergs is released in a few seconds, followed by an afterglow in all parts of the electromagnetic spectrum. Although not observed yet, theory suggests that the first generation of stars is a likely candidate for providing the progenitors of GRBs. In this article we will derive the GRB-rate for a dark matter halo at a redshift z . By using the Press-Schechter formalism we ask ourselves the question what the probability is that such a halo existed at that particular redshift. We will also derive a luminosity function for the afterglow following the actual GRB. The latter luminosity function will be compared with the sensitivities of the near infrared (NIR) camera on the upcoming James Webb Space Telescope (JWST). Finally we will try to infer whether we expect to find a GRB afterglow in a random field of the latter telescope.

1 Introduction

In 1963, during the cold war, a Nuclear Test Ban Treaty (NTBT) was signed by the governments of the USSR, the USA and the UK. This treaty prohibited the testing of nuclear devices in the atmosphere as well as in space. The USA wanted to make sure that the other countries involved did not violate the treaty and therefore they launched the Vela-satellites. These were satellites equipped with γ , X-ray and neutron detectors. In this way nuclear activities in the atmosphere or in space would certainly be detected. However, the fourth version of the satellites detected a serie of γ -flashes that did not have the characteristics of nuclear activities on earth. It was only later on, when the satellites were able to determine directions for the events, that these γ -flashes turned out to have a cosmic origin.

The discovery of GRBs in the late sixties was declassified in the beginning of the seventies. This lead to a burst of publications by astronomers wondering what was causing these γ -flashes. For a long time astronomers could not agree whether these flashes had a cosmological or a galactic origin.

In 1990 the Compton Gamma-Ray Observatory was launched. This satellite was equipped with the Burst And Transient Source Experiment (BATSE), an instrument that was able to monitor almost the entire sky for γ -flashes. It turned out that GRBs were randomly distributed across the sky, strongly favoring the theory of a cosmological origin. However, a lot of astronomers still believed that GRBs had their origin in the galactic halo because there

were no events known that could be linked to the energies involved when a GRB is placed at a cosmological distance. The final answer to this question had to wait until 1997. In this year the BeppoSax satellite discovered X-Ray counterparts of GRBs. A fairly accurate position could be determined from these observations. This enabled astronomers to search for counterparts in other parts of the spectrum, finally leading to the first redshift determination of $z = 0.8$ for a GRB. This was clearly the end of the galactic scenario: GRBs have a cosmological origin. And moreover, there was a lot of work to do for theoretical astrophysicists.

There are two classes of GRBs: short duration ($< 2s$) and long duration ($> 2s$) bursts. The physical mechanisms underlying these two classes are thought to be different. It turns out that the short bursts tend to have a lower redshift distribution than the long bursts. Therefore the energies involved in the short bursts are probably less than for the long bursts. The physics behind the short bursts is still unknown. Theory suggests the merger of two neutron stars or a neutron star and a black hole. In the context of this article we are, however, mostly interested in the long duration bursts, visible up to high redshifts. At this moment the collapsar model provides us with the best explanation of long GRBs as well as their afterglows in other parts of the spectrum.

Within the collapsar model (see section 2), there are strong arguments to think that a relatively large fraction of the first generation of stars ended their lives as a GRB. The first population of stars is formed at high redshifts and because of the enormous luminosity of a GRB we should be able to detect GRBs up to these high redshifts. By now, the highest redshift that has been determined for a GRB is $z = 6.29$. However, a good spectrum from which a redshift can be derived requires more than the ability of detecting the source. Therefore making a good spectrum is easier for the nearby, apparently more luminous GRBs, than for the GRBs at higher redshifts. This might introduce a bias towards lower redshift GRBs.

In this article we will try to infer whether it is likely that we will in the near future detect the afterglow of a GRB at high redshift that can be connected to the first stars. By now, such an observational connection has not been made yet. When such observations become available, they will probably reveal a wealth of information about the formation of the first stars at the end of the dark ages.

The outline of this article is as follows. First the theoretical basis of the model will be discussed. This involves the collapsar model in section 2, the cosmology that is used in section 3 and the formation of stars and population III stars in section 4. Then we will discuss the actual model for the expected number of GRBs in a particular halo that has just started to form stars out of zero metallicity gas. This will include a model for the star formation rate in section 5 and a model for the evolution of the metallicity in section 6. In section 7 we will use these two models to derive the total number of GRBs that is expected to occur in the particular halo. We will use the Press-Schechter formalism in section 8 and a model for the afterglow spectrum in section 9 to determine in section 10 whether it is likely that we will be able to use JWST to make an observational connection between GRBs and population III stars.

Theoretical basis of the model

2 The collapsar model

2.1 Recipe for a gamma-ray burst

The collapsar model, as put forward in [22], is at the moment the most attractive theory explaining long duration GRBs as well as their afterglows. The starting-point of this model is a rapidly rotating massive star at the end of its life that has lost its hydrogen envelope. Such a star can lose its hydrogen envelope when, during its lifetime, it undergoes a Wolf-Rayet (WR) phase. A star can undergo such a WR phase when the radiation pressure of the star at some moment exceeds the gravitational force acting on the envelope of the star. This will only happen when the opacity of the outer layers of the star is sufficiently high. Since hydrogen alone does not provide such an opacity, the hydrogen envelope should at least contain a certain fraction of metals for a WR phase. Furthermore the fact that the star is massive ensures that its radiation pressure can become high enough to overcome the gravitational binding energy. A star that satisfies these two conditions is able to lose its hydrogen envelope. But why do we actually want the star to do this?

We will find the answer to the previous question if we take a closer look at another important aspect of the collapsar scenario. One of the assumptions that this scenario makes is that some sort of inner engine in the star produces a relativistic jet of particles. On its way out of the star, the relativistic jet collides with stellar material. Because of the high energy of the relativistic jet, these collisions produce a lot of high energy γ -photons: a γ -flash. At the moment that the relativistic shock breaks through the stellar surface it propagates further into the surrounding interstellar medium (ISM). Collisions of this external blast wave with gas and dust in the ISM are thought to be responsible for the afterglow in other parts of the spectrum. A typical massive star with a hydrogen envelope has a radius of hundreds to a thousand lightseconds whereas a naked helium star has a radius of only a few light seconds. If at the moment of the burst, when the relativistic jets are produced, the star has not lost its hydrogen envelope the inner engine will cease its activities before the jet can break out. In this case the star will not produce a GRB. It is for this reason that a GRB progenitor is thought to have a Wolf-Rayet phase during its life.

But what is the inner engine that produces these jets? According to the collapsar scenario, a GRB is a "failed supernova type Ib". A supernova type Ib is the phenomenon that happens at the end of the life of a massive star, when an iron core has formed and nuclear burning is not able to produce a more stable element. The internal pressure caused by this nuclear burning falls away and the star starts to collapse under its own gravity, resulting in an enormous pressure and high temperature in the stellar core. The physical processes that play a role under these circumstances allow the formation of a neutron star. This sudden collapse creates an energetic shock wave, releasing an energy of about 10^{51} ergs. However, when the mass of the star is high enough it is possible for the star to collapse directly into a black hole. In this case a shock wave as in supernova type Ib is not produced, since such a wave simply cannot escape the black hole. What happens next to the failed supernova depends on a third important ingredient of a GRB: angular momentum.

When there is not enough angular momentum present, the newly formed black hole in the stellar core will collect all the surrounding stellar material: nothing happens, at least so it will look like for an observer. When the angular momentum of the surrounding material

and the black hole is however high enough, it is possible to form a centrifugally supported system. Although material that is closest to the rotational axis of the system will still fall into the black hole, material in the equatorial plane has enough angular momentum to withstand the gravitational attraction of the black hole. A disk-like configuration is formed, in which particles in the disk are swept up to relativistic speeds. The easiest way to escape for these relativistic particles is along the rotational axis: a relativistic pair jet is formed, giving rise to a GRB followed by its afterglow.

2.2 The influence of metallicity

There are several ways in which the metallicity has its influence in the formation of a GRB. Previously we showed that according to the collapsar scenario there are three important ingredients for the formation of a GRB:

- a Wolf-Rayet phase in which the star can lose its hydrogen envelope
- angular momentum to form a disk-like configuration
- a massive star that allows the direct formation of a black hole

Each of these ingredients is influenced by the overall metallicity.

A higher metallicity increases the opacity of the outer layers of the star, making it more easy to produce a radiation-driven wind. So a WR phase that can make a star lose its hydrogen envelope is more likely to exist at a higher metallicity. However, the lower opacity of stars at a lower metallicity, makes that their radii are smaller, facilitating the breakout of a jet. And what we have not considered by now is that a stellar wind implies a loss of both mass and angular momentum, carried away by the ejected particles. The mass loss can take away the ability of a star for a direct gravitational collapse of the core into a black hole, an essential feature of the collapsar model. And a star initially endowed with enough angular momentum to support a disk, is more likely to retain this at a lower metallicity because of the reduced angular momentum loss. But what about the hydrogen envelope?

Different suggestions have been made to overcome this problem. It could be that the rotational velocities are so high that the hydrogen envelope is almost homogeneously mixed into the core [24]. This makes it possible for a single star to become a rapidly rotating helium star without the requirement of a strong stellar wind and the associated loss of mass and angular momentum. Another possibility is that the progenitor evolves in a binary system, one of the stars stripping off the hydrogen envelope of the other [6].

Finally, as we will see in section 4, the formation of high mass stars is thought to prefer a low-metallicity environment. The higher the stellar mass, the higher the probability that its core can gravitationally collapse to a black hole. Since a low-metallicity environment is thought to produce more massive stars, we may conclude that such an environment is expected to produce also more GRBs.

Combining all off these issues, we expect that GRBs prefer a low-metallicity environment. These expectations are confirmed in a model made by Yoon et al. (2006) [25]. The results of this model are shown in figure 1.

2.3 Reliability of the model

The collapsar model seems to give a good explanation for the long GRBs and its afterglows. Moreover, this model provides us with the required $\sim 10^{51}$ ergs in γ -radiation (assuming the

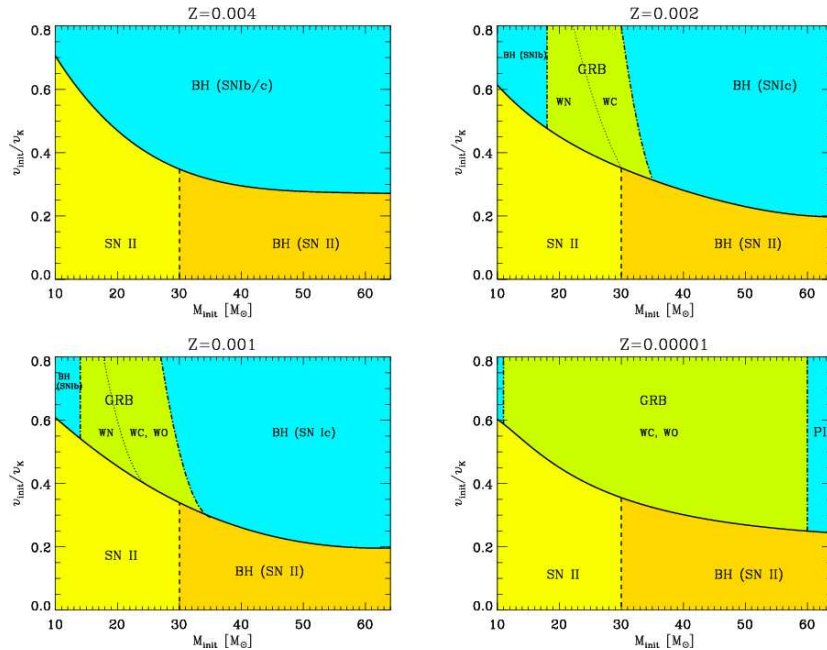


Figure 1: Model by Yoon et al. (2006) that clearly shows a metallicity dependence for the probability of making a GRB. For details on this figure see [25].

emission is not isotropic but beamed into a few percent of the sky). We should, however, not forget that the collapsar scenario is only a model. A lot of things are still uncertain and observational evidence of what the inner engine really is, does at the moment not exist.

3 Cosmology and structure formation

In this section the cosmological context that is assumed throughout this article will be discussed. It would be beyond the scope of this article to derive the formulae in this section. Therefore, we would like to refer the interested reader unfamiliar with these equations to an advanced cosmology textbook for a more detailed discussion (e.g. [16] or [19]).

3.1 Concordance model

The cosmology that we are going to use in this article is the standard Λ CDM-cosmology. This stands for an expanding flat universe that is nowadays dominated by the cosmological constant Λ and by dissipationless Cold Dark Matter. The relative size of the universe is described by the dimensionless expansion factor a , such that $a_{now} = a_0 = 1$ and $a = 0$ at the time of the Big Bang. The evolution of this expansion factor with time is given by the Friedmann equation:

$$\frac{\dot{a}^2}{a^2} = H^2 = \frac{8\pi G}{3}\rho - \frac{kc^2/R_0^2}{a^2}. \quad (1)$$

In this equation H is de Hubble parameter whereas G is the gravitational constant.

The critical density ρ_{crit} of the Universe is defined as the density for which it is just flat, in other words the critical density is the density for which $k = 0$. We can derive the critical

density through the Friedmann equation. Since for $k = 0$, we have $\rho = \rho_{crit}$, the critical density is given by:

$$\rho_{crit} = \frac{3H^2}{8\pi G}. \quad (2)$$

Furthermore, the cosmic density is specified in a dimensionless form through the density parameter Ω :

$$\Omega \equiv \frac{\rho}{\rho_{crit}} = \frac{8\pi G\rho}{3H^2}. \quad (3)$$

A particular choice of universe can be parameterized by the following set of numbers: $\{H_0, \Omega_0, \Omega_{rad,0}, \Omega_{m,0}, \Omega_{\Lambda,0}\}$. Therefore, it turns out to be convenient to rewrite the Friedmann equation in terms of these parameters:

$$dt = \frac{1}{H_0} \frac{da}{\sqrt{\Omega_{rad,0} \cdot a^{-2} + \Omega_{m,0} \cdot a^{-1} + \Omega_{\Lambda,0} \cdot a^2 + (1 - \Omega_0)}}. \quad (4)$$

In the Λ CDM-cosmology the universe is specified by $H_0 = 71 \text{ km} \cdot \text{s}^{-1} \cdot \text{Mpc}^{-1}$, $\Omega_0 = 1$, $\Omega_{rad,0} = 0$, $\Omega_{\Lambda,0} = 0.73$ and $\Omega_{m,0} = 0.27$. This universe is often referred to as the concordance model.

3.2 Present-day value of the cosmic density ρ_0

We can rewrite equation 3 for the density, taking the current values for H , Ω and ρ to obtain:

$$\rho_0 = \frac{3}{8\pi G} \Omega_0 H_0^2. \quad (5)$$

For G and H_0 we are going to use the following numbers:

- $G = 6.673 \cdot 10^{-11} \text{ m}^3 \text{ kg}^{-1} \text{ s}^{-2} = 6.673 \cdot 10^{-11} \cdot \left(\frac{1}{3.086 \cdot 10^{16}}\right)^3 \cdot 1.989 \cdot 10^{30} \text{ pc}^3 \text{ M}_{\odot}^{-1} \text{ s}^{-2}$
- $H_0 = h \cdot 100 \text{ km} \cdot \text{s}^{-1} \cdot \text{Mpc}^{-1} = h \cdot \frac{100}{3.086 \cdot 10^{19}} \text{ s}^{-1} = 0.71 \cdot \frac{100}{3.086 \cdot 10^{19}} \text{ s}^{-1}$

Filling in these numbers in equation 5, we find a present-day value of the cosmic density of $\rho_0 = 2.775 \cdot 10^{-7} \text{ M}_{\odot} \text{ pc}^{-3}$. This cosmic mass density is related to the number density (of baryons) through:

$$n_0 = \frac{\rho_0}{\mu \cdot m_p} \quad \text{and} \quad n_{b,0} = \frac{\Omega_b \cdot \rho_0}{\mu \cdot m_p}. \quad (6)$$

In this μ denotes the reduced mass of the gas particles whereas Ω_b is the mass percentage of baryonic matter. The latter is according to the concordance model $\frac{0.04}{0.27} = 14.8\%$. Note that the first equation is not completely correct, since we do not know anything about the nature of dark matter (so we can in fact not relate this to a number density). However, for the formation of stars we will only consider baryonic matter so that this is not an important issue.

3.3 Hierarchical clustering

The early universe consisted of an almost homogeneous density field in which some tiny fluctuations were present. Nowadays the universe reveals a lot of structure, at the smaller scales being far from homogeneous. How did such a complex variety of structures form out of the initially simple, almost homogeneous density field? In essence, the answer is simple: gravity.

The initial overdensity field can be represented by a Gaussian distribution. The only way in which dark matter can interact is through the always attractive force of gravity. This means that although the overdensities were very small in the early universe, matter in underdense regions started to move to overdense regions. When overdensities reach a critical value relative to the background density, they can decouple from the Hubble flow and may start to collapse. The smallest halos of dark matter are thought to form first, continuously merging together to form larger and larger halos: hierarchical clustering. The abundance of halos with a certain mass M_{halo} at a redshift z can be calculated on the basis of a model. In this article we are going to use a model that is similar to the Press-Schechter formalism [18].

The mass percentage of baryonic matter is according to the concordance model 14.8%. This means that the amount of baryonic matter is low compared to the amount of dark matter. The gravitational potential wells in the universe are therefore mainly formed by the dark matter halos. In the hierarchical clustering scenario, baryonic matter is thought to follow the potential wells created by the dark matter halos. This baryonic matter inside the dark matter halos is the material out of which eventually the first stars will form. And it is the formation of these first stars that in some sense mark the transition from the simple homogeneous early universe to the highly structured one as we see it nowadays.

4 Population III stars

4.1 Star formation

Nowadays stars are born in cold dense gas clouds that consist primarily of molecular hydrogen with a relatively small mass fraction of metals and other molecules. These systems are known as molecular clouds. In the cores of these clouds typical values of temperature and density are $T \sim 10\text{ K}$ and $n \sim 10^6\text{ cm}^{-3}$. Under these circumstances, certain regions of these clouds may start to collapse under their own gravity because their masses become too high to retain virial equilibrium. This is a particular state of a cloud in which it is neither contracting due to gravity nor expanding due to its internal pressure, in this case the virial theorem applies:

$$2 \cdot E_{kinetic} + E_{potential} = 0. \quad (7)$$

Assuming a spherically symmetric cloud with radius R , we can derive what variables play a role in establishing virial equilibrium. The gravitational potential energy of a spherically symmetric cloud is given by:

$$E_{potential} = - \int_0^R \frac{GM(r)}{r} \rho(r) \cdot 4\pi r^2 \cdot dr. \quad (8)$$

One more assumption we make in this analysis is that the density is constant throughout the cloud, such that $\rho(r) = \rho$. The total mass of the cloud is therefore given by $M = \frac{4\pi}{3} \rho R^3$

whereas the mass inside a radius r is represented by $M(r) = \frac{4\pi}{3}\rho r^3$. Using this in equation (8) gives us:

$$E_{potential} = - \int_0^R \frac{(4\pi)^2}{3} G \rho^2 r^4 dr = - \frac{3GM^2}{5R}. \quad (9)$$

At the typical temperature of a molecular cloud, rotational and vibrational modes of molecular hydrogen do not contribute to the internal energy of the gas. This is because the smallest rotational transition has an energy of $\sim k_B \cdot 512K$, where $k_B = 1.38 \cdot 10^{-23} JK^{-1}$ is the Boltzmann constant. The internal kinetic energy of a gas consisting completely of molecular hydrogen, is therefore given by:

$$E_{kinetic} = \frac{3}{2} N k_B T = \frac{3}{2} \left(\frac{M}{2m_H} \right) k_B T. \quad (10)$$

Applying the virial theorem, as defined in equation (7), results in the following condition for the mass of the cloud:

$$M_J = \sqrt{\frac{3}{4\pi}} \left(\frac{5k_B}{2Gm_H} \right)^{\frac{3}{2}} \rho^{-\frac{1}{2}} T^{\frac{3}{2}} \propto \rho^{-\frac{1}{2}} T^{\frac{3}{2}}. \quad (11)$$

This critical mass for which the cloud is in virial equilibrium is called the Jeans mass. If the mass of the cloud exceeds the Jeans mass, it starts to collapse. Obviously equation (11) does not provide us with the exact value of the Jeans mass. A spherically symmetric cloud with constant density where other physical phenomena, like magnetic fields and angular momentum, do not play a role is what we may call a rather unique configuration. However, it does at least show us how the Jeans mass depends on the density and the temperature in the cloud. Note that the same dependencies can be derived by setting the free-fall time equal to the sound crossing time. A more insightful way to write equation (11) is the following:

$$M_J \approx 0.73 M_\odot \cdot \left(\frac{n}{10^6 cm^{-3}} \right)^{-\frac{1}{2}} \left(\frac{T}{10K} \right)^{\frac{3}{2}}. \quad (12)$$

This equation shows us that for a typical molecular cloud with a temperature of $10 K$ and a density of $10^6 cm^{-3}$, the Jeans mass is approximately $0.73 M_\odot$.

What happens to a cloud with $M > M_J$ after it started to collapse depends on the characteristics of the cloud. Collisional excitations of particles in the cloud will, in the case of radiative de-excitations, lead to the production of photons. When the cloud is optically thin to this radiation, it can escape from the cloud. In this particular case the photons, carrying with them some energy, allow the cloud to cool. If the cooling rate is high enough, it can enable an isothermal collapse so that the cloud can enter a phase of runaway collapse. However, when the cloud is optically thick to this radiation the collapse will be almost adiabatic. The temperature increases in this case and therefore the Jeans mass may also increase when the density does not increase fast enough. So a cloud must be able to cool if it wants to enter a phase of runaway collapse. This condition is expressed in a physical way by demanding that the cooling time t_{cool} is shorter than the free-fall time t_{ff} .

We conclude that a cloud that has both $M > M_J$ and $t_{cool} < t_{ff}$ will enter a phase of runaway collapse until some other force stops the contraction. When the density inside the center of the cloud becomes high enough, an optically thick hydrostatic core is formed. Now this core is not able to cool anymore so that the temperature will increase. Yet this does not stop the collapse of the cloud, because the surrounding material is still able to cool and

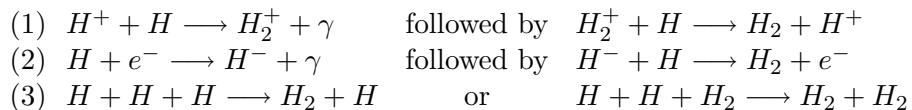
collapse. This material will compress the core further and it will also partially accrete onto the optically thick core. At some point the temperature and density in the core become so high that hydrogen atoms start to fuse together and form helium. The outward pressure produced by this process blows away the surrounding material: a new star is born.

4.2 Molecular hydrogen cooling in the first stars

The physics of the formation of the first stars is in fact a lot simpler than star formation physics nowadays. By definition there are no other stars that influence the environment (e.g. by radiation, winds or supernovae), we do not expect the presence of strong magnetic fields and the primordial gas consisted mainly of hydrogen with some helium and lithium. Moreover the initial conditions of the formation of the first stars are prescribed by the cosmology that is described in section 3.

It is primarily the chemical composition of the primordial gas that makes the first, so-called population III stars, different from population I and II stars that are formed in normal star formation. The presence of metals and molecules in star forming regions nowadays, enable cooling to temperatures on the order of $\sim 10 K$. This is due to the low energy-spacings of fine-structure transitions in metals and especially the vibrational and rotational levels in molecules. But when the first stars formed these metals and molecules were not present. The only way in which such a cloud can initially cool is by atomic hydrogen cooling. The lowest energy spacing available in atomic hydrogen is about $\sim k_B \cdot 10^4 K$. It turns out that the virial temperatures of the halos in which the first stars formed were below this threshold of $10^4 K$ for atomic hydrogen cooling. Cooling is therefore only possible if the cloud can produce a species with a lower energy-spacing. And the only species with a lower energy-spacing that can form out of hydrogen atoms without nuclear reactions (for this you need stars) is molecular hydrogen.

The formation of molecular hydrogen in the early universe is hampered by the absence of dust. This makes that initially H_2 molecules are formed in the gas phase. There are three important formation channels for H_2 molecules in the gas phase [7]:



The corresponding reaction rates make that formation channel (1) is unimportant in comparison with formation channel (2). At redshifts higher than $z \approx 200$ however the H^+ formation channel is important because at that time CMB photons are energetic enough to destroy H^- ions, which makes this formation channel impossible. But since the dark matter halos in which the first stars are thought to form were not there yet at that time, this is not important for our purpose. The last formation channel, the so-called three-body reactions, is a very efficient one but only at densities in excess of 10^8 cm^{-3} . It is therefore the second formation channel that determines how much molecular hydrogen is formed in a particular cloud. Tegmark et al. (1997) [20] have set up a model for a low density environment that takes into account both formation channel (1) and (2). As a rule of thumb they conclude that if the temperature of the protostellar cloud is high enough to produce a molecular hydrogen fraction on the order of $5 \cdot 10^{-4}$, then a gas cloud with $M > M_J$ will collapse.

As was already mentioned the lowest lying rotational transition of molecular hydrogen has an energy spacing of $k_B \cdot 512 K$. The average energy of each particle is $\frac{3}{2}k_B T$, so that

at a temperature of $\sim 340\text{ K}$ the average particle would not have enough energy anymore to collisionally excite the lowest rotational level. However the energies of the particles are distributed according to the Maxwell-Boltzman distribution, and collisions with the high energy tail of this distribution allow cooling by molecular hydrogen to proceed to a temperature of $\sim 100 - 200\text{ K}$.

4.3 When did the first stars form?

So in order to obtain a fraction of molecular hydrogen that is high enough to enable a gas cloud to cool, the host dark matter halo has to have a certain virial temperature T_v . That is, the fraction of molecular hydrogen that is formed in a gas cloud depends on the temperature since the reaction rates in this formation process increase with temperature. But what determines the virial temperature of a dark matter halo?

A dark matter halo is in virial equilibrium when the virial theorem, equation (7), holds. In the same way we derived the Jeans mass as a condition for hydrostatic equilibrium in a spherical gas cloud with constant density ρ and temperature T , we can derive what the virial temperature T_v of a spherical dark matter halo with constant density ρ and mass M_{halo} has to be in order to be in hydrostatic equilibrium. Rewriting equation (11) for the Jeans mass, thereby replacing T by T_v and M_J by M_{halo} allows us to derive an expression for the virial temperature:

$$T_v = \left(\sqrt{\frac{3}{4\pi}} \right)^{\frac{2}{3}} \left(\frac{5k_B}{2Gm_H} \right) \rho^{\frac{1}{3}} M^{\frac{2}{3}} \propto M^{\frac{2}{3}} \cdot \rho^{\frac{1}{3}}. \quad (13)$$

The density of a virialized halo can be expressed in units of the cosmic density as $\rho_{vir} = \delta\rho_c$. This expression turns out to be very useful because one can derive that a virialized spherical dark matter halo has an overdensity of $\delta = 18\pi^2 \approx 178$ with respect to the background density ρ_c . Equation (13) tells us that the virial temperature depends on the virial density and since the virial density depends on the cosmic density this implies that the virial density is redshift dependent:

$$T_v \propto M^{\frac{2}{3}} \cdot \rho^{\frac{1}{3}} \propto M^{\frac{2}{3}} \cdot a^{-1} \propto M^{\frac{2}{3}} \cdot (1+z). \quad (14)$$

Baryonic gas that falls into a dark matter potential well, will in first instance have a kinetic temperature that is equal to the virial temperature of the halo. Virial temperatures of 10^4 K or higher will of course allow Lyman- α cooling although the cooling rate will initially be relatively slow since the densities n involved are still small and the cooling rate scales with n^2 for low densities. Assuming the virial temperature of the halo determines the kinetic gas temperature of the cloud, it is essentially this virial temperature that determines the fraction of molecular hydrogen that is produced. Since we derived previously that there is a minimum fraction of H_2 molecules required to enable a gas cloud to cool, it is therefore the virial temperature that determines whether a dark matter halo can successfully host a protostar. This virial temperature in turn depends on the mass of the halo, M_{halo} , and its virialization redshift z_{vir} . So in order to answer the question when the first stars formed, we actually have to answer the question when there was for the first time a combination of halo mass and virialization redshift $\{M_{halo}, z_{vir}\}$ that had a virialization temperature that was high enough to produce enough molecular hydrogen to enable a gas cloud in the halo to cool. This idea is nicely illustrated by a model of Tegmark et al. (1997) [20]. The results of this model are shown in figure 2. Assuming that the first stars formed in a 3σ mass fluctuation,

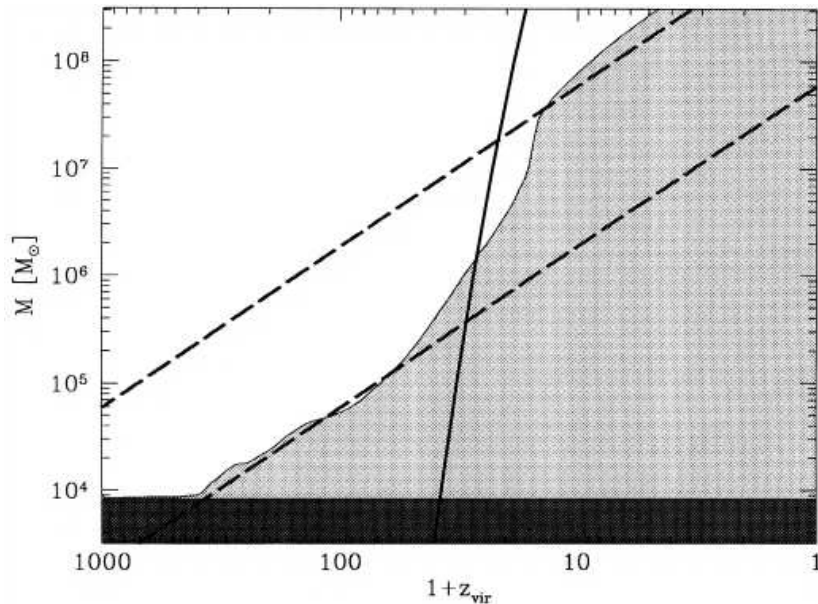


Figure 2: Results of a model by Tegmark et al. (1997) [20] that determines for a given redshift z_{vir} the required mass M needed for collapse. Only halos with parameters $\{z_{vir}, M\}$ that lie above the shaded area have a virial temperature that is high enough to produce a sufficient fraction of molecular hydrogen for a gas cloud inside the halo to cool. The dashed straight lines correspond to virial temperatures of $10^3 K$ and $10^4 K$. The dark shaded region does not enable efficient radiative cooling because in these regions the required virial temperature is lower than the temperature of the Cosmic Microwave Background (CMB) radiation. The solid line represent a mass fluctuation of 3σ , assuming a standard normalized CDM model for structure formation as described in section 3.

this figure shows us that the first dark matter halo in which a gas cloud could collapse formed at a redshift of $z = 30$ and had a mass of $M_{halo} = 2 \cdot 10^6 M_{\odot}$.

Note that at temperatures above $3000 K$ H_2 -molecules are collisionally destroyed. The regime between 3000 and $10000 K$ is therefore in fact unstable. On the one hand a small increase in the H_2 fraction will enable the cloud to cool to a temperature below $3000 K$, preventing the destruction of the coolant, whereas on the other hand a small decrease in the H_2 fraction will allow the temperature to increase, enhancing the destruction of H_2 -molecules. The latter vicious circle will continue until the cloud reaches a temperature of $10^4 K$, the equilibrium point at which $Ly-\alpha$ cooling becomes important again.

4.4 The formation of the first stars

An Initial Mass Function (IMF) describes the mass distribution of newly formed stars. An IMF does not specifically describe how many stars are formed per mass bin per unit time, but it describes the form $\frac{dN}{dM}$ of this mass distribution. The model that we develop in this article requires the use of such an IMF for population III stars. However, before we turn to this we first want to know what the characteristic mass scale is of a population III star and we will discuss whether fragmentation of the primordial gas cloud will play an important role.

4.4.1 Characteristic mass scale

A characteristic mass scale of collapse is obviously the Jeans mass. In equation (12) we derived that for star formation nowadays the Jeans mass under typical circumstances is $\sim 0.73 M_{\odot}$. A characteristic mass scale of a primordial protostellar cloud can be derived by determining the typical Jeans mass. For this, we need to know what we expect to be the typical temperature and density in such a cloud. We have already seen that cooling by molecular hydrogen cannot proceed under $\sim 100 - 200 K$, therefore we take $150 K$ as a typical temperature. A characteristic density can also be determined by taking a closer look at the cooling process. When densities n are low, each collision in the gas cloud results almost instantaneously in a radiative decay. That is, collisional de-excitations are not important. In this case the cooling rate is proportional to n^2 . However, when the density reaches some critical value $n_c \approx 10^4 cm^{-3}$, collisional deexcitations start to compete with radiative de-excitations. Since collisional deexcitations do not cool the gas, the cooling process is suddenly less efficient and the cooling rate is now proportional to n (see [21] for more details on cooling processes). Once the cloud reaches this critical density it enters a phase of quasi-hydrostatic equilibrium due to the now inefficient cooling process. It is at this point where the mass of the cloud should exceed the Jeans mass in order to move away from this phase and enter a phase of runaway collapse. This argument makes that we take $n = n_c \approx 10^4 cm^{-3}$ as the typical density in a primordial gas cloud. This typical state of a primordial gas cloud is in agreement with results as obtained with hydrodynamical numerical simulations by [1] and [2].

Deriving the Jeans mass as previously in equation (11), only now for a spherically symmetric cloud with constant density that consists completely out of hydrogen atoms results in the following characteristic mass scale of the parent gas cloud out of which the first stars formed:

$$M_J \approx 1693 M_{\odot} \cdot \left(\frac{n}{10^4 cm^{-3}} \right)^{-\frac{1}{2}} \left(\frac{T}{150 K} \right)^{\frac{3}{2}}. \quad (15)$$

This mass of the parent clump out of which the first star formed already provides us with an upper limit for the mass of the population III star. The final mass of the star is however not determined by this. When the collapse of the cloud continues, the density of the central core will at some moment become $\sim 10^8 cm^{-3}$. As was mentioned before, at this point the three-body formation channel for hydrogen becomes efficient and when the density increases to $\sim 10^{10} cm^{-3}$ the inner $1 M_{\odot}$ is able to become almost completely molecular. This causes a sudden boost in cooling that may lead to thermal instabilities of the cloud that can cause fragmentation. Like in normal star formation, the density at the center of the cloud will at some moment become so high that it becomes optically thick. Simulations (e.g. by [14]) have shown that the optically thick hydrostatic core, that forms at a density of $10^{22} cm^{-3}$, has a mass of $5 \cdot 10^{-3} M_{\odot}$. This is essentially the same as in present-day star formation. So does population III star formation not differ from normal star formation? Yes it does, because the final mass of the star is not determined by the mass of this central core but by the amount of material that can accrete onto this central core. This in turn, depends on the accretion rate.

The total amount of material that is available for accretion is set by the Jeans mass. The time it takes for a Jeans mass to accrete is given by the free fall time, a characteristic time of collapse. For a spherical halo the freefall time is given by:

$$t_{ff} = \sqrt{\frac{3\pi}{32G\rho}} \propto \rho^{-\frac{1}{2}}. \quad (16)$$

Dividing the Jeans mass from equation (11) by the free fall time from equation (16) shows us that the accretion rate depends strongly on temperature:

$$\dot{M}_{acc} \approx \frac{M_J}{t_{ff}} \propto T^{\frac{3}{2}}. \quad (17)$$

Since the typical temperature in a primordial protostellar cloud is about fifteen times larger than nowadays, we conclude that the accretion rate in such a cloud is about $15^{\frac{3}{2}} \approx 60$ times larger than in ordinary star formation. Therefore population III stars are in general thought to be very massive ones. In normal star formation the accretion process is halted when a Wolf-Rayet wind blows away the surrounding material. However, by definition during the formation of the first stars there were no metals and dust that could drive such a wind. Is it then possible that a population III star accretes all the material of the surrounding gas cloud? In that case the upper bound of the mass of a population III star would be a one or two thousand solar masses, the Jeans mass of the gas cloud. But we have to take into account the fact that these stars are very massive, which implies that their lifetimes are very short. Assuming that accretion cannot proceed longer than this lifetime, the upper bound for the mass of a population III is by [3] derived to be $\sim 500 M_{\odot}$.

4.4.2 Fragmentation

It is not sure that the collapsing primordial protostellar clouds continue their collapse until a star forms. In fact there are several reasons to expect the development of instabilities in the cloud. These instabilities can give rise to fragmentation, breaking the cloud up in different parts and consequently lowering the available mass to accrete onto the star.

When the three-body formation channel for molecular hydrogen becomes efficient, the central part of the cloud undergoes a sudden boost in cooling. This can possibly cause a thermal instability in the cloud. Such an instability would also require the presence of initial density perturbations in the cloud. However, if these density perturbations were present during the slowly collapsing phase around $n \sim n_c$ they would have been erased by pressure forces at this time. Moreover, compressional heating will prevent the cloud from experiencing a sudden drop in temperature.

Another important seed for further fragmentation of the cloud is angular momentum. The protostellar cloud starts with a given amount of angular momentum, in general for early star formation this amount is thought to be relatively small. If the collapse continues and the radius of the cloud decreases, conservation of angular momentum implies that the typical rotational velocities of the cloud increase. This can lead to a centrifugally supported configuration that inhibits further accretion onto the core but it can also cause fragmentation of the cloud. Note that angular momentum transport, by for example turbulent viscosity or gravitational torques in binary systems, can allow the protostellar cloud to lose angular momentum during its collapse. This can prevent the cloud from fragmentation.

Different simulations (e.g. [1], [2], [27]) showed that further subfragmentation of the cloud does not take place. These results make that we will ignore the possibility of subfragmentation in the rest of this article.

4.4.3 Initial mass function of population III stars

In present-day star formation the IMF is often described by a Salpeter mass function:

$$\frac{dN}{dM} = \xi'_0 \cdot M^{-2.35}. \quad (18)$$

In this equation the stellar masses M are thought to vary between $0.1 M_\odot < M < 100 M_\odot$. Unfortunately such a prescription does not exist for population III stars, a consequence of the fact that we have not been able yet to observe these stars. However, since the model we develop in this article requires that we have such a prescription we are forced to make some rough assumptions at this point.

Different simulations have shown that the formation of a $100 M_\odot$ star is easily feasible under the circumstances of population III star formation. On the other hand the lifetimes of these stars give rise to an upper boundary of $500 M_\odot$. This leads to the first assumption that the mass range of population III stars is given by $100 M_\odot < M < 500 M_\odot$. Do we expect the IMF to follow a particular shape? As far as we know now there is no reason why for example a $200 M_\odot$ star would be more favourable to form than a $400 M_\odot$ star. Therefore we assume that, in the assumed mass range, the IMF of population III stars is a flat one:

$$\frac{dN}{dM} = \xi_0. \quad (19)$$

4.5 Feedback mechanisms

Once a first generation of stars has formed, they probably influence their environment in several ways. The fact that they were very massive implies on the one hand that they emitted a lot of high energy photons into their environment and on the other hand that the associated short lifetimes of these stars will enable them to produce a supernova-like phenomenon shortly after their birth. This takes care of the first enrichment of the universe with heavy elements.

The production of these heavy elements raises the overall metallicity of the environment quickly. We already saw that population III star formation differs from ordinary star formation in the sense that it takes place in a zero-metallicity environment. Therefore the raise of the overall metallicity associated with the death of a population III star may lead to a transition in the IMF from the early top heavy one to the normal Salpeter IMF as is observed nowadays. This transition takes place as soon as the overall metallicity reaches the so-called critical metallicity. The critical metallicity is thought to vary between $10^{-5} Z_\odot$ and $10^{-3} Z_\odot$ [15]. In this article we will use the value of $Z_{crit} \sim 10^{-3.5} Z_\odot$ derived by [4].

4.6 Population III stars as GRB progenitors

Comparing sections 2 and 4 makes clear that population III stars have some properties that make them favourable progenitors of GRBs. That is, population III stars have a low metallicity and they are thought to be very massive. On the other hand, the formation of population III stars requires the cloud not to have too much angular momentum, to prevent it from fragmentation, whereas a GRB requires, according to the collapsar model, a sufficient amount of angular momentum to form a disk. A GRB that is produced by a population III star should therefore have a carefully balanced amount of angular momentum.

With the assumption that a certain fraction η_{GRB} of the total generation of first stars is able to produce a GRB as in the collapsar scenario, it is now time to start the development of a model.

Description of the model

5 Star formation rate in a dark matter halo

We start setting up a model by considering the star formation rate in a dark matter halo. For this, we assume that population III stars follow an IMF as described by equation (19). We normalize the IMF by using the Schmidt-law. From this we will derive a star formation rate per unit area as a function of stellar mass, a function that describes how many stars inside a mass bin dM around M are formed per unit time per unit area in a particular halo.

5.1 Schmidt-law

The Schmidt-law describes for a given column density of gas, what the star formation rate per unit area is in solar masses per year. It is then the IMF that tells you how the total amount of star formation $\Sigma_{SFR} \cdot \Delta t$ is distributed over the different stellar masses.

The Schmidt-law is given by (observationally determined in [11]):

$$\Sigma_{SFR} = 2.5 \cdot 10^{-4} \left(\frac{\Sigma_{gas}}{M_{\odot} pc^{-2}} \right)^{1.4} M_{\odot} yr^{-1} kpc^{-2}. \quad (20)$$

Theoretically, we expect the star formation rate to be proportional to the density divided by the free-fall time. Since the free-fall time $t_{ff} \propto n^{-0.5}$, we expect a $\Sigma_{SFR} \propto \Sigma_{gas}^{1.5}$ dependence of the star formation rate on the density. Note that this power of 1.5 lies within the confidence level of the observationally determined density dependence of $\Sigma_{SFR} \propto \Sigma_{gas}^{1.4}$. We are going to use the observationally derived power of 1.4 because the theoretically derived one follows from a simple argument that does not take everything into account that might play a role.

5.2 Normalization of the IMF

The condition for correctly normalizing the IMF with the Schmidt-law is:

$$\int \frac{dN}{dM} \cdot M \cdot dM = \Sigma_{SFR} \cdot \Delta t. \quad (21)$$

For our population III IMF this results in the following normalization condition:

$$\xi_0 = 2.0525 \cdot 10^{-9} \left(\frac{\Sigma_{gas}}{M_{\odot} pc^{-2}} \right)^{1.4} \cdot \Delta t. \quad (22)$$

The number of stars dN that are formed within the mass bin dM per unit time per unit area is now given by:

$$\frac{dN}{dA \cdot dt} = 2.0525 \cdot 10^{-9} \left(\frac{\Sigma_{gas}}{M_{\odot} pc^{-2}} \right)^{1.4} \cdot dM. \quad (23)$$

As we can see, this formation rate of stars within a mass bin dM is a function of the surface mass density Σ_{gas} . It is therefore important that we derive an expression for this surface mass density.

5.3 The column density in a collapsed halo

5.3.1 Density of baryons after the collapse

A Dark Matter halo decouples from the Hubble flow at a relative overdensity of $\frac{n}{n_c} = \delta = 178$ according to [13]. At the moment of decoupling, the density of the complete halo is given by $n = n_c \cdot \delta$, in which n_c is the cosmic density at the moment of decoupling. Note that in the case of matter the cosmic density evolves as $n_c = n_0 \cdot a^{-3} = n_0 \cdot (1+z)^3$ in which n_0 is the cosmic density nowadays. So the density in the halo at the moment of decoupling is

$$n = \delta \cdot n_0 \cdot (1+z)^3. \quad (24)$$

However, the things we are going to derive relate to baryonic matter (since we want to know which stars and how many of these stars are formed). This brings in two important factors that we have to take in account. First the density of baryonic matter is only a fraction Ω_b of the total mass density. As a second point we also have to take into account that baryonic matter is able to collapse. We are going to assume spherical collapse with a collapse factor $\lambda^{-1} = \frac{R_{initial}}{R_{final}}$. Since for matter $n \propto R^{-3}$, we have $\frac{n_{initial}}{n_{final}} = \frac{R_{final}^3}{R_{initial}^3} = \lambda^3$. Putting these two factors together, we get the following final density of baryonic matter after the collapse:

$$n_b = \delta \cdot \lambda^{-3} \cdot \Omega_b \cdot n_0 \cdot (1+z)^3. \quad (25)$$

Because we are more interested in GRB that happened at high redshifts, we are mainly concerned with halos in the early universe. Baryonic matter will in general not have collapsed to a disk at this time. Therefore, we make the assumption that that the collapse is completely spherical.

5.3.2 Converting density into a column density

However, for using the Schmidt-law we need to know the column density. We assume that the rate of star formation will depend on the column density that corresponds to the longest column in the halo. In the case of complete spherical collapse, the longest column is the one through the center with a length of two times the radius of the sphere. For getting the corresponding column density N , we have to multiply the density with the length that we want to consider, in this case two times the radius R . For the mass of the spherical halo we have:

$$M_{halo} = \frac{4\pi}{3} \cdot \rho \cdot R^3 = \frac{4\pi}{3} \cdot n \cdot \mu \cdot m_p \cdot R^3. \quad (26)$$

We can rewrite this equation to obtain the radius of the sphere,

$$R = \left(\frac{4\pi}{3}\right)^{-\frac{1}{3}} \cdot \left(\frac{M_{halo}}{\mu m_p}\right)^{\frac{1}{3}} \cdot n^{-\frac{1}{3}}. \quad (27)$$

Note that $n = \frac{n_b}{\Omega_b}$, so that the column density N_b of baryons corresponding to a density n_b as given in equation (25) is:

$$N_b = 2 \cdot n_b \cdot R = \left(\frac{\pi}{6}\right)^{-\frac{1}{3}} \cdot \left(\frac{M_{halo}}{\mu m_p}\right)^{\frac{1}{3}} \cdot \Omega_{b,g}^{\frac{1}{3}} \cdot n_b^{\frac{2}{3}} = \left(\frac{\pi}{6}\right)^{-\frac{1}{3}} \cdot \delta^{\frac{2}{3}} \cdot \lambda^{-2} \cdot \Omega_{b,g} \cdot \left(\frac{M_{halo}}{\mu m_p}\right)^{\frac{1}{3}} \cdot n_0^{\frac{2}{3}} \cdot (1+z)^2. \quad (28)$$

Typical values in this context are:

- $\delta = 178$
- $\lambda = 0.07$
- $\Omega_b = 0.148$

5.4 The star formation rate

5.4.1 Surface mass density

As we can see in equation (23), the number of stars $\frac{dN}{dA \cdot dt}$ in the mass bin dM that is formed per unit area per unit time depends on the surface mass density Σ_{gas} of the halo whereas equation (28) only provides us with a number density N_b . These two quantities are related to each other through:

$$\Sigma_{gas} = N_b \cdot \mu \cdot m_p. \quad (29)$$

Combining this equation with equations (6) and (28) results in the following expression for the surface mass density:

$$\Sigma_{gas} = \left(\frac{\pi}{6}\right)^{-\frac{1}{3}} \cdot \delta^{\frac{2}{3}} \cdot \lambda^{-2} \cdot \Omega_{b,g} \cdot M_{halo}^{\frac{1}{3}} \cdot \rho_0^{\frac{2}{3}} \cdot (1+z)^2. \quad (30)$$

5.4.2 Star formation rate

Finally, now that we have an expression for the surface mass density Σ_{gas} from equation (30), we can use equation (23) to determine what the star formation rate of stars with mass M per unit area, $\frac{dN}{dA \cdot dt}$, is as a function of halo mass and redshift for our population III IMF. This results in the following expression:

$$\frac{dN}{dA \cdot dt} = 2.0525 \cdot 10^{-9} \left(\frac{\left(\frac{\pi}{6}\right)^{-\frac{1}{3}} \cdot \delta^{\frac{2}{3}} \cdot \lambda^{-2} \cdot \Omega_{b,g} \cdot M_{halo}^{\frac{1}{3}} \cdot \rho_0^{\frac{2}{3}} \cdot (1+z)^2}{M_{\odot} \text{ pc}^{-2}} \right)^{1.4} \cdot dM. \quad (31)$$

Filling in the constants in this equation reduces the equation to:

$$\frac{dN}{dA \cdot dt} = 1.811 \cdot 10^{-11} \cdot M_{halo}^{\frac{1.4}{3}} \cdot (1+z)^{2.8} \cdot dM. \quad (32)$$

More interesting is, however, the formation rate $\frac{dN}{dt}$ of stars within the mass bin dM in the complete halo. For this we have to multiply equation (32) with the area A of the halo. The assumption that the halo is spherical in combination with the radius from equation (27), the number density in the halo from equation (25) and the cosmic number density from equation (5) results in the following surface area of the halo:

$$A_{halo} = \pi R^2 = \pi^{\frac{1}{3}} \cdot \lambda^2 \cdot \left(\frac{4}{3} \cdot \delta \cdot \Omega_{b,g} \cdot n_0\right)^{-\frac{2}{3}} \cdot \left(\frac{M_{halo}}{\mu m_p}\right)^{\frac{2}{3}} \cdot (1+z)^{-2} = 15.72 M_{halo}^{\frac{2}{3}} \cdot (1+z)^{-2} \text{ pc}^2. \quad (33)$$

The combination of equation (32) and (33) gives us the total number of stars with mass M that are formed per unit time in a halo with mass M_{halo} at redshift z ,

$$\frac{dN}{dt} = 2.848 \cdot 10^{-16} \cdot M_{halo}^{\frac{17}{15}} \cdot (1+z)^{0.8} \cdot dM. \quad (34)$$

6 Metallicity evolution and mixing processes

Each supernova or GRB has a certain metallicity yield. Therefore, as more of these explosions take place, the overall metallicity of the halo increases. This rise in metallicity has two consequences for the number of GRBs in the halo. First, at a certain metallicity the IMF transforms from a population III IMF to a Salpeter IMF (this is thought to happen at a metallicity of $\sim 10^{-3.5}Z_{\odot}$). After this IMF transition, the metallicity is still low enough to enable the production of GRBs (although star formation now takes place with a Salpeter IMF). From figure 1 we can conclude that at a metallicity of $\sim 10^{-2}Z_{\odot}$ it is not possible anymore to produce GRB in an efficient manner. Therefore at this metallicity there is a cutoff in the number of GRB.

6.1 Metallicity-yields

When we want to know how the metallicity in a halo evolves with time, we first need to know how many metals are produced at the end of the life of a star with mass M . For this, we need to know how a star with mass M ends its life. An overview of this distribution of stellar end-products is found in figure 3. In the mass range of population III stars, stars in the ranges $100M_{\odot}$ - $140M_{\odot}$ and $260M_{\odot}$ - $500M_{\odot}$ will directly form a black hole. Although these stars produce a certain amount of metals, only a very small fraction of this will be injected into the environment and help to raise the overall metallicity. Most of the metals that are produced in these stars will be locked in the black holes that form directly after their deaths. In the context of metal production, we will assume that stars that directly form a black hole do not contribute to the overall metallicity. This implies that for population III stars only stars in the mass range $140 - 260 M_{\odot}$ are important for determining the metallicity evolution of a halo. As can be seen in figure 3, stars in this mass range end their lives as a Pair Instability Supernova (PISN).

6.1.1 Pair Instability Supernovae

The more massive a star is, the hotter it is. And since stars radiate almost like a perfect black-body, these hotter more massive stars will produce more energetic γ -photons. At some point, the most energetic photons have energies on the order of $E \sim 2m_e c^2 \sim 1MeV$. According to the mass-energy equivalence, such a photon has enough energy to produce an electron-positron pair. This newly formed pair will quickly annihilate and form a new γ -photon.

Normally, the more energetic a γ -photon the larger its mean free path (since the photoelectric effect and Compton scattering are less efficient for high energy photons). However, when gamma-rays become energetic enough to form electron-positron pairs, the mean free path of the γ -photons will start to increase again. This increase in the mean free path causes an instability. As a consequence the temperature increases, producing more high energy photons and hence amplifying the instability. For stars with a mass larger than $\sim 140M_{\odot}$, the released thermal energy by pair-productions is larger than the gravitational binding energy of the star. A PISN is produced and its progenitor is completely disrupted. Important in this is that the mass of the remnant is $M_{rem} = 0$, therefore all the metals that are produced in a PISN are ejected into the halo causing a significant increase in the overall metallicity. To determine the evolution of the metallicity, we need to have a function $y_m(M)$ that gives the fraction of the stellar mass M that is converted into metal m .

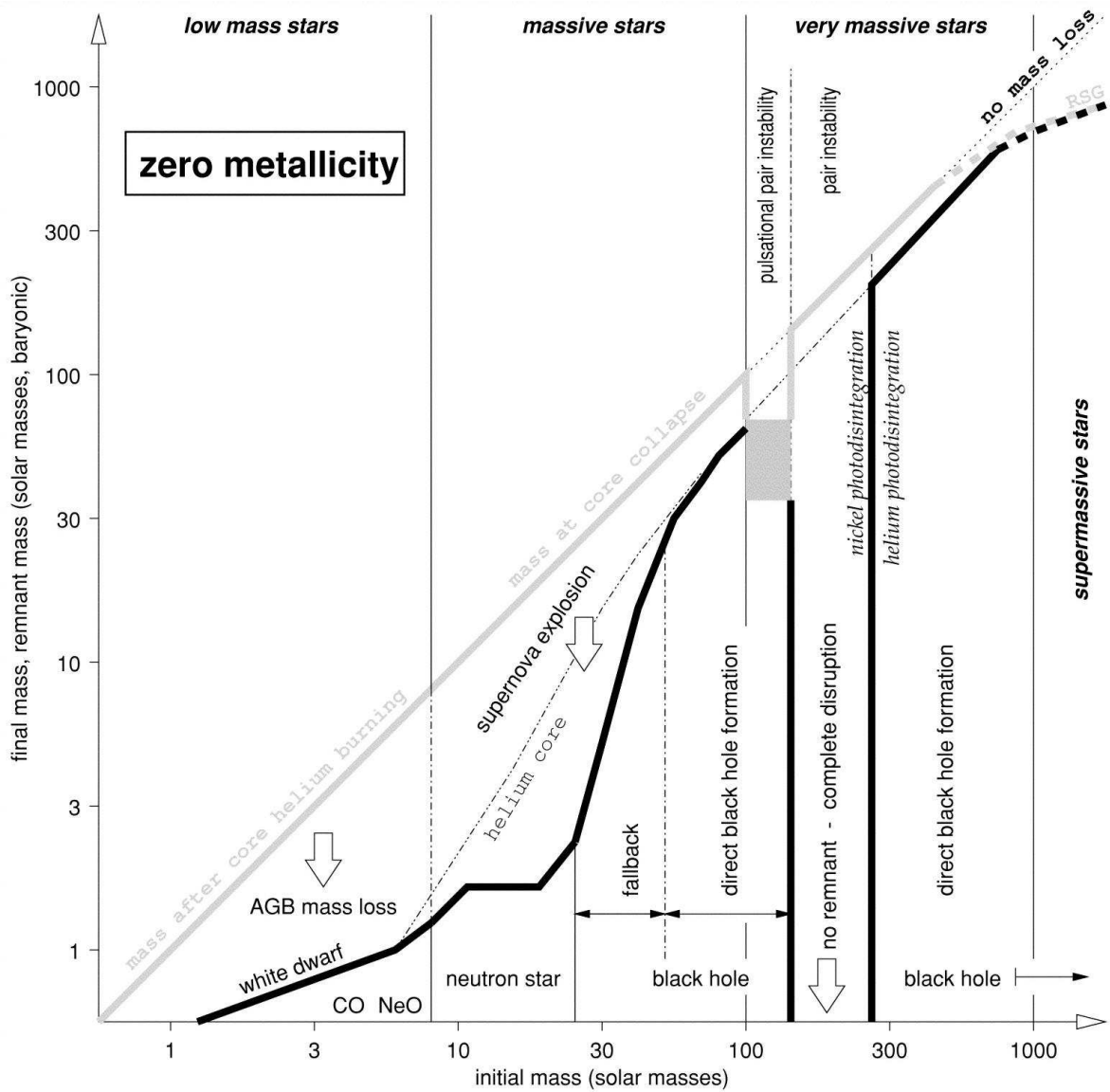


Figure 3: This figure shows that stars with an initial mass between $100M_{\odot}$ and $140M_{\odot}$ will directly form a black hole. The same holds for stars with an initial mass that is higher than $260M_{\odot}$. Supernova explosions or GRBs that are directly followed by the formation of a black hole are of no importance for us here since they do not pollute their environments with metals: almost all the metals that are formed are locked in the black hole. However, between $140M_{\odot}$ and $260M_{\odot}$ the life of a star is ended with a PISN. Such an explosion leaves no remnant behind and therefore all the metals that are produced during such an explosion are available to increase the metallicity of the halo. In the study of the metallicity evolution of the halo we therefore need to take a closer look at these explosions. Figure from [8].

Table 1: Carbon yields

mass He-core (M_{\odot})	stellar mass (M_{\odot})	carbon-yield (M_{\odot})	fraction of total stellar mass
65	140.0	6.89	4.9%
70	149.2	4.54	3.04%
75	158.5	4.32	2.73%
80	167.7	4.33	2.58%
85	176.9	4.28	2.42%
90	186.2	4.21	2.26%
95	195.4	4.13	2.11%
100	204.6	4.01	1.96%
105	213.8	3.85	1.80%
110	223.1	3.74	1.68%
115	232.3	3.73	1.61%
120	241.5	3.71	1.54%
125	250.8	3.61	1.44%
130	260.0	3.49	1.34%

Carbon yields for different masses of the central helium core. The corresponding total stellar mass is derived with the assumption there is a linear relation between the mass of the helium core and the total mass. The last column represents the carbon yield as a fraction of the total stellar mass.

6.1.2 Carbon enrichment of a halo

In this article we will use metallicity yields as presented in [8]. This article provides a model that determines for different stellar masses in the PISN-range the yields for a set of metals. In this, it is not the total mass of the star but the mass of the helium core that is taken as a variable starting-point. This is because the mass of this core determines the maximum temperature of the star. Previously we already concluded that the total stellar mass range of PISN is given by $140M_{\odot}$ - $260M_{\odot}$. In [8] the mass range of the helium core varies between $65M_{\odot}$ - $130M_{\odot}$. In this article the assumption is that there is a linear relation between the mass of the central helium core and the total mass of the star.

In considering the metallicity evolution of the halo we will take the carbon yields in PISN and relate these to the solar abundance. The solar abundance of carbon, which we define here as the mass fraction of carbon, is $Z_{C\odot} = 0.0041$. Table 1 presents the carbon yields for the different masses of the helium cores that are used in [8]. The corresponding stellar mass, with the assumption that there is a linear relation between the mass of the helium core and the total stellar mass, is also mentioned in table 1.

The only problem is that table 1 provides us with a set of discrete values whereas we would like to have a continuous function $y_C(M)$ that gives us the carbon yields of a star with mass M as the fraction of the total stellar mass. Such a function can, in a rather simple way, be implemented in the formalism we developed in section 5. In order to get such a function, we have used MATLAB to make a fit to the dataset as presented in table 1. This fit is presented in figure 4, and results in the following yield function for carbon:

$$y_C(M) = 2.5104 \cdot 10^{-6}M^2 - 0.0012104M + 0.16062. \quad (35)$$

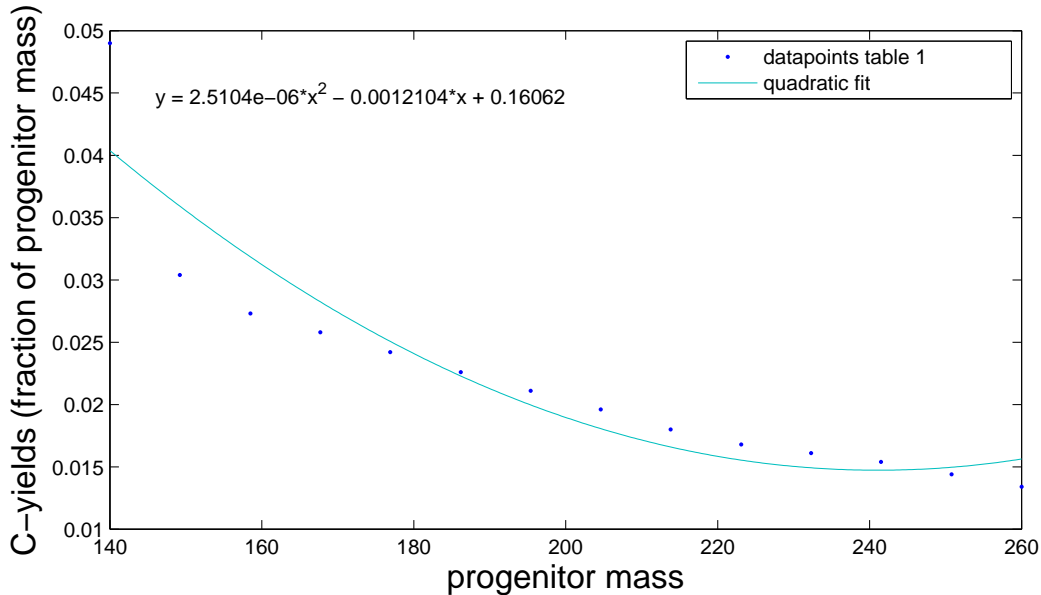


Figure 4: Quadratic fit to the dataset presented in table 1. This fit is made with MATLAB.

Now that we have the function $y_C(M)$ for the stars that are thought to produce a PISN, and therefore eject all their metals in the environment, we can derive how many of these stars are required to raise the overall metallicity to the critical value of $10^{-3.5}Z_\odot$.

The formation rate from equation (32) gives us the number of stars in the mass bin dM that are formed in a halo with mass M_{halo} at redshift z per unit time. When we multiply this equation with the absolute carbon yield $y_C(M) \cdot M$ we obtain the amount of carbon $\frac{dC}{dt}$ in solar masses that is produced in a halo with mass M_{halo} at redshift z per unit time by stars within a mass range dM around M :

$$\frac{dC}{dt} = 2.848 \cdot 10^{-16} \cdot M_{halo}^{\frac{17}{15}} \cdot (1+z)^{0.8} \cdot M \cdot (2.5104 \cdot 10^{-6} M^2 - 0.0012104 M + 0.16062) \cdot dM. \quad (36)$$

The total rate $\frac{dC_{total}}{dt}$ at which carbon is ejected into the halo is obtained by integrating equation (36) over the mass range of PISN:

$$\frac{dC_{total}}{dt} = \int_{140M_\odot}^{260M_\odot} 2.848 \cdot 10^{-16} \cdot M_{halo}^{\frac{17}{15}} \cdot (1+z)^{0.8} \cdot M \cdot (2.5104 \cdot 10^{-6} M^2 - 0.0012104 M + 0.16062) \cdot dM. \quad (37)$$

Evaluating the integral over the stellar mass range results in:

$$\frac{dC_{total}}{dt} = 1.417 \cdot 10^{-13} \cdot M_{halo}^{\frac{17}{15}} \cdot (1+z)^{0.8} M_\odot \cdot yr^{-1}. \quad (38)$$

6.1.3 How long does it take to produce enough metals to reach the critical metallicity?

The final thing we want to know is how long it takes a halo to reach the critical metallicity of $10^{-3.5}Z_\odot$. Equation (38) is, however, not a straightforward equation that enables us to

determine this time. In fact, the only thing we can do with equation (38) is determine the total amount of carbon C_{total} that is produced between two times t_1 and t_2 by integrating over time:

$$C_{total} = \int_{t_1}^{t_2} 1.417 \cdot 10^{-13} \cdot M_{halo}^{\frac{17}{15}} \cdot a^{-0.8} \cdot dt. \quad (39)$$

The integral in equation (39) is not a trivial one to evaluate. This is because the redshift z and the dimensionless expansion factor a are time-dependent variables. The relation between these variables is given by equation (4) and we can use this equation together with the concordance model to rewrite equation (39) as:

$$C_{total} = \int_{a_1}^{a_2} 1.417 \cdot 10^{-13} \cdot M_{halo}^{\frac{17}{15}} \cdot a^{-0.8} \cdot \frac{1}{H_0} \frac{da}{\sqrt{0.27 \cdot a^{-1} + 0.73 \cdot a^2}}. \quad (40)$$

So equation (40) enables us to determine the total amount of carbon that is ejected into the halo between the values a_1 and a_2 or equivalently $\frac{1}{(1+z_1)}$ and $\frac{1}{(1+z_2)}$ of the dimensionless expansion factor. Taking a dark matter halo with mass M_{halo} at a redshift z_{begin} with zero metallicity as our starting-point, we would like to know the redshift at which it reaches a metallicity of $10^{-3.5} Z_{\odot}$. Analytically this is not a feasible thing to determine from equation (40). Therefore we have written a MATLAB program that starts with the initial state just discussed, subsequently takes small steps in redshift space and compares the obtained metallicity with the desired value. As soon as the critical metallicity is reached the program gives the redshift z_{end} at which this happens as output value. Once the program has determined this value, the total number of PISN N_{PISN} that was required to enrich the halo to the required value can be determined by evaluating the following integral:

$$N_{PISN} = 2.848 \cdot 10^{-16} \int_{1/(1+z_{begin})}^{1/(1+z_{end})} \int_{140M_{\odot}}^{260M_{\odot}} M_{halo}^{\frac{17}{15}} \cdot \frac{1}{H_0} \frac{a^{0.8}}{\sqrt{0.27 \cdot a^{-1} + 0.73 \cdot a^2}} \cdot dM \cdot da. \quad (41)$$

6.1.4 Results

Now it is time to present some results of the MATLAB program we have written. We have taken different values for the total halo mass M_{halo} and for the redshift z_{begin} at which the halo formed. From this starting point, the redshift z_{end} at which the critical metallicity was reached is determined. The time between z_{begin} and z_{end} is determined with equation (4). Subsequently the total number of PISN that were needed to enrich the halo to the critical value is determined with equation (41). For different halo masses the results of these calculations are presented in table 2.

6.2 Mixing model

The final thing that our model should provide us with is the number of GRBs that can be produced in a particular halo before the overall metallicity reaches a value that is equal to the critical value. What do the result presented in table 2 tell us in this context? According to this table a halo with a total mass of $10^7 M_{\odot}$ only needs one PISN to produce enough carbon to raise the overall metallicity to the critical metallicity. But does this imply that at this point the halo reaches the overall critical metallicity? It certainly need not. Obviously, at the moment this first PISN takes place, the metals that are ejected are not homogeneously distributed over the halo. Locally the metallicity reaches the critical value. When we want

Table 2: Number of PISN before reaching the critical metallicity at $z = 25$

M_{halo}	$time(years)$	$number\ of\ PISN$
$10^6 M_{\odot}$	21533	0.1
$10^7 M_{\odot}$	16149	1.1
$10^8 M_{\odot}$	11535	10.8
$10^9 M_{\odot}$	8459	107.5
$10^{10} M_{\odot}$	6229	1076
$10^{11} M_{\odot}$	4614	10834

This table presents the number of PISN that is needed to reach the critical metallicity at $z = 25$. Note that for the lighter halos the binding energy can be on the order of the energy of one supernova. In this case one supernova is able to destroy the complete halo. Furthermore, if we want to use the time that is needed to produce enough metals to reach the critical metallicity as the time to reach an overall metallicity that is equal to the critical metallicity, we should realize that we have to build in a delay of $\sim 10^6$ years. This is the estimated lifetime of the first stars, in the case of a continuous star formation process it is only at this time that stars start to produce eject metals into their environment.

to know when the overall metallicity of the halo reaches this value, we also have to model the mixing process that distributes the metals over the halo.

A PISN is thought to produce a shock wave that propagates through the halo. It is this shock wave that is responsible for the distribution of the metals in the halo. We make the assumption that there exists a universal shock velocity v_{shock} , this assumption enables us to model the metal distribution in a rather simple way. The shock velocity of a supernova is in [21] described as:

$$v_s(t) = 250 \left(\frac{t}{t_0} \right)^{-5/7} km\ s^{-1} \quad (42)$$

In this, a typical normalization time is $t_0 \sim 2 \cdot 10^4$ year. As we will see a typical mixing time for a halo is on the order of 10^6 year so that a typical shock will start with a velocity of $250\ km \cdot s^{-1}$ and end with a velocity of $\sim 15\ km \cdot s^{-1}$. To facilitate the calculations we take $v_{shock} = 50\ km \cdot s^{-1}$ as a universal shock velocity, the so-called snowplough velocity.

Imagine that at a particular moment in time there have been N PISN. We assume that these PISN are distributed homogeneously over the halo and that the mean distance between two PISN is L_{PISN} . Now we can define the characteristic mixing time scale T_{mix} of the halo as follows:

$$T_{mix} = \frac{L_{PISN}}{v_{shock}} = \frac{R_{halo}}{\sqrt[3]{N} \cdot v_{shock}}. \quad (43)$$

In this equation the radius of the halo R_{halo} can be determined with equation (27).

6.3 When does a halo reach the critical metallicity?

We have now developed two conditions that should be fulfilled before the halo reaches the critical metallicity. On the one hand it should have produced enough metals and on the other hand the time between the moment the halo begins to produce PISN and the moment the critical metallicity is reached should at least be equal to the characteristic mixing time scale.

The second condition will also be build into the model. For this, we have made a MATLAB program that first determines (like in section 6.1) the number of PISN that are required

to produce enough metals and the time T_{PISN} it takes to produce this number of PISN. Subsequently the program determines the characteristic mixing time scale T_{mix} of the halo at that particular moment in time. Note that this mixing time scale changes when more PISN are produced. The program will now compare T_{PISN} and T_{mix} .

When T_{PISN} is larger than T_{mix} , the program takes the value of T_{PISN} as the time it takes the halo to reach the critical metallicity. When T_{PISN} is smaller than T_{mix} , the program takes another step in redshift space. It determines again what the number of PISN is in the halo and calculates the corresponding mixing time. Now this mixing time is compared with the total time T since the halo started to produce PISN. This loop continues until the mixing time T_{mix} grows larger than the total time T . At the moment this happens, the total time T is taken as the time it takes the halo to reach the critical metallicity. The model is now able to determine how long a particular zero-metallicity halo with mass M_{halo} that starts to produce stars at $z = z_{begin}$ continues to form population III stars. That is, at the moment the halo reaches the overall critical metallicity the IMF is assumed to make a transition to a Salpeter IMF that is found in normal star forming regions.

Although a Salpeter IMF is also able to produce GRB progenitors, we will not consider this here. This is mainly because we expect that GRBs do not form in an environment with an overall metallicity higher than $10^{-2}Z_{\odot}$. The halos that we modeled did all have a mixing time that was larger (at least one order of magnitude except for the halos with a mass $10^6 M_{\odot}$) than the time needed to produce sufficient metals. In fact at the moment the total time becomes equal to the mixing time, the amount of metals that had been produced is sufficient to reach the cut-off metallicity of $10^{-2}Z_{\odot}$. This, in combination with the fact that a Salpeter IMF is less likely to produce GRB progenitors, brings us to the assumption that once the IMF makes the transition to a Salpeter IMF the contribution to the cosmological GRB signal becomes modest.

7 The GRB rate in a dark matter halo

The final thing that the model should provide us with is the GRB rate in a particular dark matter halo. For this we are going to assume that a certain fraction η_{GRB} of all supernovae produce a GRB. The value for this fraction is empirically derived for intermediate redshift GRBs by [12] to be $\eta'_{GRB} = 0.001$. However, as was explained previously we think that GRBs are more likely to occur at the end of the life of a population III star. Since there are no observations of population III stars available, using the fraction η'_{GRB} of present-day star formation can be a serious underestimate. Therefore we take the value $\eta_{GRB} = 0.005$ that is found as the global fraction of supernovae over GRBs in the model developed by [25].

The fact that the assumed population III IMF produces only very massive stars has two consequences. First, all of these stars will end their life with a supernova-like event. Second, these stars die almost immediately after their birth. These two things brings us to the approximation that the supernova-rate in a particular halo is equal to the star formation rate. Under this assumption, the GRB rate in a halo is given by:

$$\frac{N_{GRB}}{dt} = 2.848 \cdot 10^{-16} \left(\int_{100M_{\odot}}^{140M_{\odot}} dM + \int_{260M_{\odot}}^{500M_{\odot}} dM \right) \eta_{GRB} \cdot M_{halo}^{\frac{17}{15}} \cdot a^{-0.8}. \quad (44)$$

Since we do now also know how long it takes for a halo, that begins to form stars at z_{begin} , to reach the critical metallicity for a transition of the IMF at z_{end} , we can derive the total

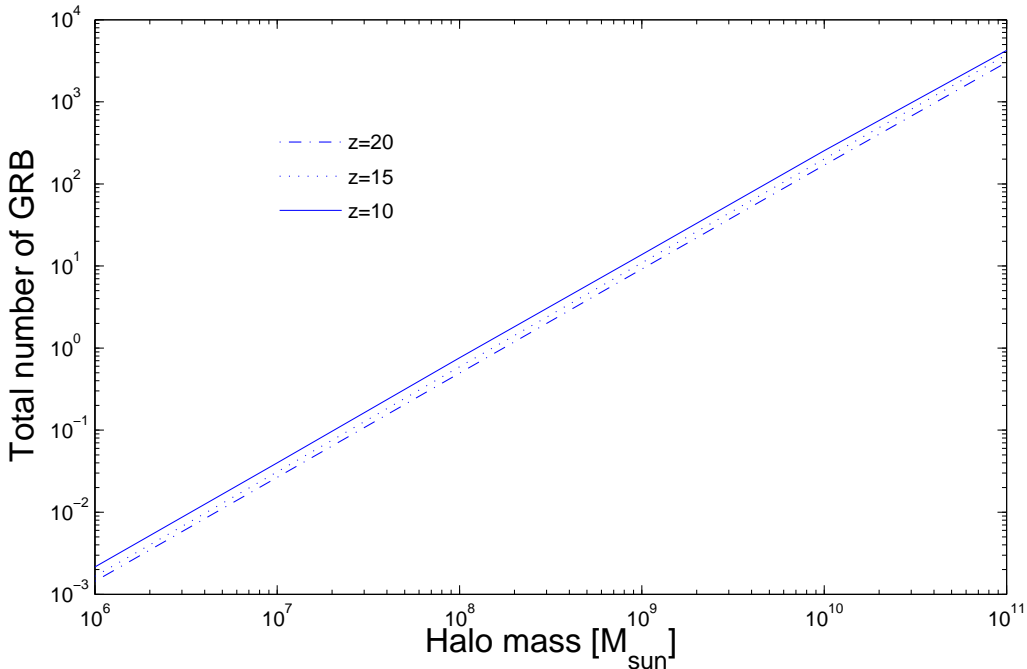


Figure 5: The total number of GRBs that according to our model occurs in a particular halo. This number is determined for formation redshifts of $z = 20$, $z = 15$ and $z = 10$. The slope of the lines turns out to be ~ 1.26 . On the basis of equation (45) one would expect a slope of $\frac{17}{15} \approx 1.13$. The discrepancy between the expected and the real slope is caused by the dependence of z_{end} on the total mass of the halo.

number of GRB that took place in the halo during its population III stage. Note that we made the assumption that all stars in the mass range $140 - 260 M_{\odot}$ form a PISN so that these cannot form a GRB. The total number of GRB that take place in a halo is according to our model therefore given by:

$$N_{GRB} = 3.9872 \cdot 10^{-16} \cdot M_{halo}^{\frac{17}{15}} \cdot \int_{1/(1+z_{begin})}^{1/(1+z_{end})} \frac{1}{H_0} \frac{a^{-0.8} \cdot da}{\sqrt{0.27 \cdot a^{-1} + 0.73 \cdot a^2}}. \quad (45)$$

The results of this model are shown in figure 5.

8 The distribution of dark matter halos

Now that we know for a particular dark matter halo how long the phase of population III star formation lasts and how many GRBs are produced during this phase it is time to ask ourselves the question how likely it is to find this particular halo at a given redshift. For answering this question we adopt a hierarchical clustering scenario described by a simple form of the Press-Schechter formalism. This Press-Schechter formalism describes the distribution of dark matter halos with mass M_{halo} as a function of redshift with the assumption that the primordial density fluctuations were Gaussian.

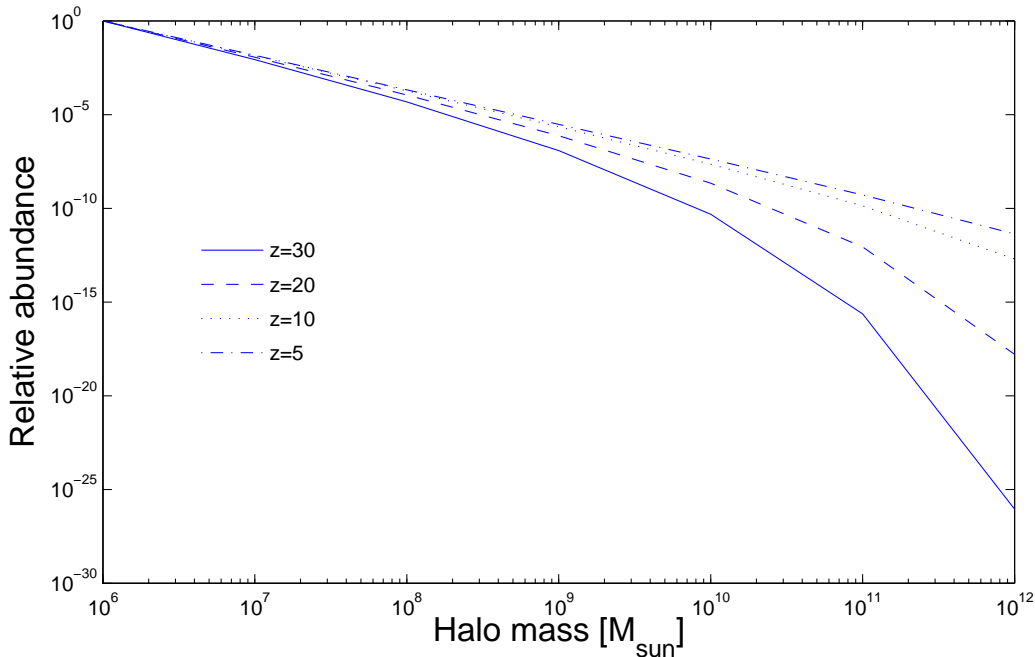


Figure 6: The relative abundance of dark matter halos as compared with the abundance of halos with a mass of $M = 10^6 M_\odot$

In this article we will use the Press-Schechter formalism as described in [13]. According to this article the distribution of dark matter halos is given by:

$$n(M, z) = \left(\frac{2}{\pi}\right)^{\frac{1}{2}} \cdot \left(\frac{\rho_i}{M^2}\right) \cdot y \cdot \frac{d \log y}{d \log M} \cdot e^{\frac{-y^2}{2}}. \quad (46)$$

In this equation $y = \delta_c(1+z)/\sigma(M)$ where $\delta_c = 1.68$ and $\sigma(M) = 16.3b^{-1}(1 - 0.3909r_0^{0.1} + 0.4814r_0^{0.2})^{-10}$. In this r_0 is the initial radius of collapse in units of Mpc and given by $r_0 = (M/10^{12} M_\odot)^{1/3} \cdot (\Omega h^2)^{-1/3}$ whereas ρ_i is the initial density given by $\rho_i = 178 \cdot \rho_0 \cdot (1+z)^3$.

8.1 Relative halo abundances

Equation (46) gives a prescription for the number of halos with mass between M and $M + dM$ that is expected in $1 Mpc^3$. Although one can use this equation to obtain the number of halos in a certain volume, it is particularly useful to compare the abundance of halos with different masses. That is, $\frac{n(M_1, z)}{n(M_2, z)}$ tells you how many halos with mass M_1 you expect to find for each halo with mass M_2 at a given redshift z . Figure 6 shows the abundance of dark matter halos relative to the abundance of dark matter halos with $M = 10^6 M_\odot$. One can clearly see that this plot satisfies the scenario of hierarchical clustering, as with decreasing redshift the relative abundance of more massive halos grows considerably.

Motivated by cosmological simulations of population III star formation (e.g. [1] or [2]), we make the assumption that halos of $10^6 M_\odot$ acquire for the first time a significant abundance at a redshift of $z = 30$. The relative abundances in figure 6 enable us now to say something about the abundances of halos with a higher mass.

8.2 The expected number of halos in a field on the sky

Another useful thing to derive in the context of the distribution of halos, is the number of halos that we expect in a certain field on the sky between redshifts z_1 and z_2 .

The angular size $\Delta\theta$ of such a field is related to the physical size $d(z)$ at redshift z through the angular diameter distance D_A :

$$d(z) = D_A \cdot \Delta\theta = \frac{D_c(z)}{1+z} \cdot \Delta\theta. \quad (47)$$

In this $D_c(z)$ represent the comoving distance corresponding to redshift z and is defined as:

$$D(z) = \frac{c}{H_0} \int_{\frac{1}{1+z}}^{a_0} \frac{da}{\sqrt{0.27 \cdot a^{-3} + 0.73}}. \quad (48)$$

The volume element dV that corresponds to a field of $\Delta\theta \times \Delta\theta$, that substends a solid angle $d\Omega$ on the sky, between z and $z + dz$ or alternatively a and $a + da$ is now given by:

$$dV(z) = d(z)^2 \cdot dD(z) = \left(\frac{c}{H_0} \int_{\frac{1}{1+z}}^{a_0} \frac{da}{\sqrt{0.27 \cdot a^{-3} + 0.73}} \right)^2 \cdot d\Omega \cdot \frac{c}{H_0} \frac{da}{\sqrt{0.27 \cdot a^{-3} + 0.73}}. \quad (49)$$

The number of halos $dN(M)$ with mass between M and $M + dM$ that we expect to find in this volume element is $dN(M) = n(M, z) \cdot dV$. The total number of halos $N(M)$ with mass between M and $M + dM$ that we expect to find in our field of $\Delta\theta \times \Delta\theta$ between redshift z_1 and z_2 is given by:

$$N(M) = \int_{z_1}^{z_2} n(M, z) \cdot dV(z). \quad (50)$$

We will not show the complete formula here since this will be a rather unattractive one. Instead we will now use a MATLAB program to calculate what the expected number of halos in a mass bin dM around M is in a field of $1' \times 1'$. The results of this calculations are shown in figure 7.

9 A model for the spectrum of a GRB

If we want to determine whether it is possible to detect a GRB at a particular redshift, we need to know the emission spectrum. This spectrum can be divided into the spectrum of the instantaneous burst and the spectrum of the afterglow emission. Although the spectrum of the instantaneous burst is far more energetic than that of the afterglow, it is the latter spectrum that is of interest to us. This is because the instantaneous burst lasts for only a few seconds in the source frame. Despite the time dilation in the observers frame, the chance that a telescope is pointed at this field at the particular time of the instantaneous burst is very small. Note that this is not the case with satellites like BeppoSax that can monitor almost the entire sky.

Moreover, the regime of high-energy photons is not the one that gives you the best spectral resolution. Although photons are redshifted, the high energy photons that can have energies of a few keV will never end up in for example the infrared window of the upcoming JWST with its excellent sensitivity. This favours the afterglow of a GRB to reveal a lot of information about the environment in which the first stars formed. For this reason, we have to model this afterglow spectrum so that we can infer whether it is likely that we will in the near future detect an afterglow of a population III GRB.

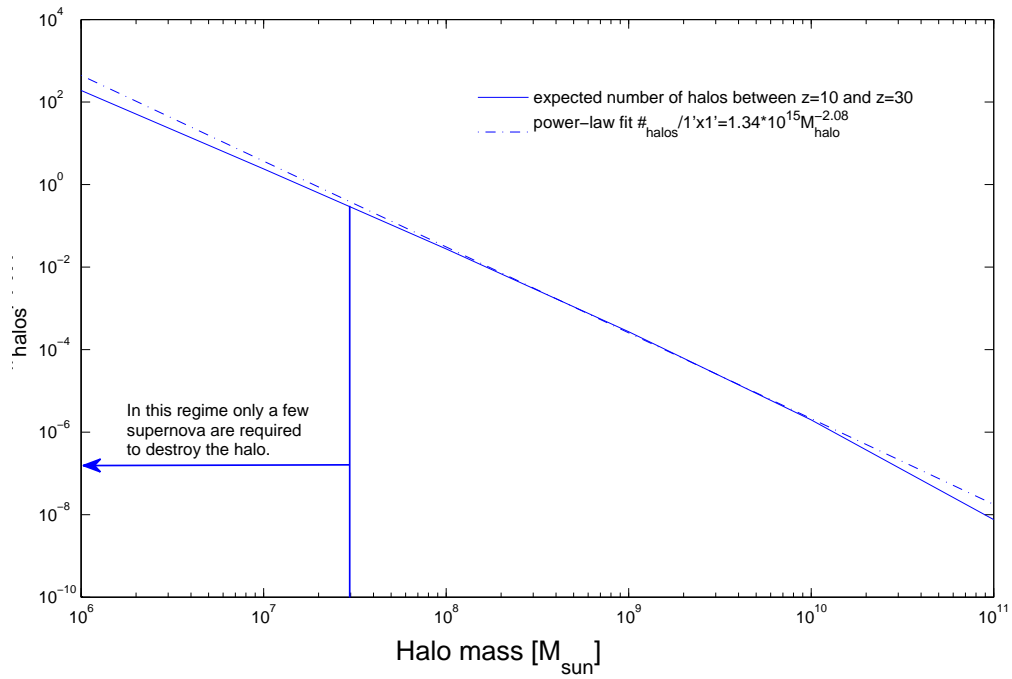


Figure 7: Number of halos inside a mass bin of dM around M that we expect to find in a field of $l' \times l'$ in redshift space between $z = 10$ and $z = 30$. This number of halos can be fitted by an power-law which will later on turn out to be useful.

9.1 The afterglow spectrum

The afterglow of a GRB is thought to be caused by a relativistic shock wave from the GRB. Therefore we can model the spectrum of the afterglow as synchrotron emission from a decelerating relativistic shock wave as in [5], for the details on these emission mechanism we refer the reader to this article.

The synchrotron emission that is responsible for the afterglow is caused by relativistic electrons that have a power-law distribution of Lorentz factors γ_e , with a minimum Lorentz factor of γ_m . Furthermore γ_c is a threshold Lorentz factor below which electrons do not lose a significant amount of energy to synchrotron radiation. If $\gamma_m > \gamma_c$, all electrons do lose a lot of energy to the production of synchrotron emission. This will cause the total population of electrons to cool down rapidly to $\gamma_e \sim \gamma_c$. When $\gamma_c > \gamma_m$, only electrons with $\gamma_e > \gamma_c$ will cool down rapidly. This threshold Lorentz factor divides the emission by synchrotron processes into two regimes. If $\gamma_m > \gamma_c$, the flux as observed in the observers frame is according to this model [5] given by:

$$F_\nu = F_{\nu m} \begin{cases} (\nu/\nu_c)^{1/3} & \nu_c > \nu, \\ (\nu/\nu_c)^{-1/2} & \nu_m > \nu \geq \nu_c, \\ (\nu_m/\nu_c)^{-1/2} \cdot (\nu/\nu_m)^{-p/2} & \nu \geq \nu_m. \end{cases} \quad (51)$$

If on the other hand $\gamma_c > \gamma_m$, the synchrotron afterglow spectrum as observed in the observers frame is given by:

$$F_\nu = F_{\nu m} \begin{cases} (\nu/\nu_m)^{1/3} & \nu_m > \nu, \\ (\nu/\nu_m)^{-(p-1)/2} & \nu_c > \nu \geq \nu_m, \\ (\nu_c/\nu_m)^{-(p-1)/2} \cdot (\nu/\nu_c)^{-p/2} & \nu \geq \nu_c. \end{cases} \quad (52)$$

The value for the power-law index p is taken from [10] to be $p = 2.2$, since this value is a more recent one than the one used in [5]. In these spectra $F_{\nu m}$ is the observed peak flux whereas ν_c and ν_m are the characteristic synchrotron frequencies described above. According to [5], for a fully adiabatic shock, these are given by:

$$\begin{aligned} \nu_c &= 2.7 \cdot 10^{12} \epsilon_B^{-3/2} \cdot E_{52}^{-1/2} \cdot n_1^{-1} \cdot t_d^{-1/2} \cdot (1+z)^{-1/2} & Hz \\ \nu_m &= 5.7 \cdot 10^{14} \epsilon_B^{1/2} \cdot \epsilon_e^2 \cdot E_{52}^{1/2} \cdot t_d^{-3/2} \cdot (1+z)^{1/2} & Hz \\ F_{\nu m} &= 1.1 \cdot 10^5 \epsilon_B^{1/2} \cdot E_{52} \cdot n_1^{1/2} \cdot d_{28}^{-2} \cdot (1+z) & \mu Jy \end{aligned} \quad (53)$$

In this, ϵ_B and ϵ_e are the fractions of the shock energy that are converted to, respectively, magnetic fields and the acceleration of electrons. The values for these two constants are also taken from [10] and turn out to be $\epsilon_B = 0.01$ and $\epsilon_e = 0.1$. E_{52} is the energy of the shock in 10^{52} ergs, n_1 the density in cm^{-3} , t_d the time in days in the observers frame between the observation of the afterglow and the actual GRB and d_{28} the luminosity distance in $10^{28} cm$.

In this the luminosity distance is a redshift-dependent quantity that can be determined for a concordance model with the following equation:

$$d_L = (1+z) \cdot D = (1+z) \cdot c \cdot \int_{t_e}^{t_o} \frac{dt}{a(t)} = (1+z) \cdot \frac{c}{H_0} \int_{a_e}^{a_0} \frac{da}{\sqrt{0.27 \cdot a + 0.73 \cdot a^4}}. \quad (54)$$

When we now consider for example a GRB at redshift $z = 20$ with an energy of 10^{52} ergs, determine the luminosity distance with equation (54) and take for the density of the gas the baryonic density of the halo from equation (25) we can compute a set of synchrotron spectra for the afterglow. These spectra are shown in figure 8. Note that these spectra are not corrected for possible extinction mechanisms, due to the dust in the host galaxies.

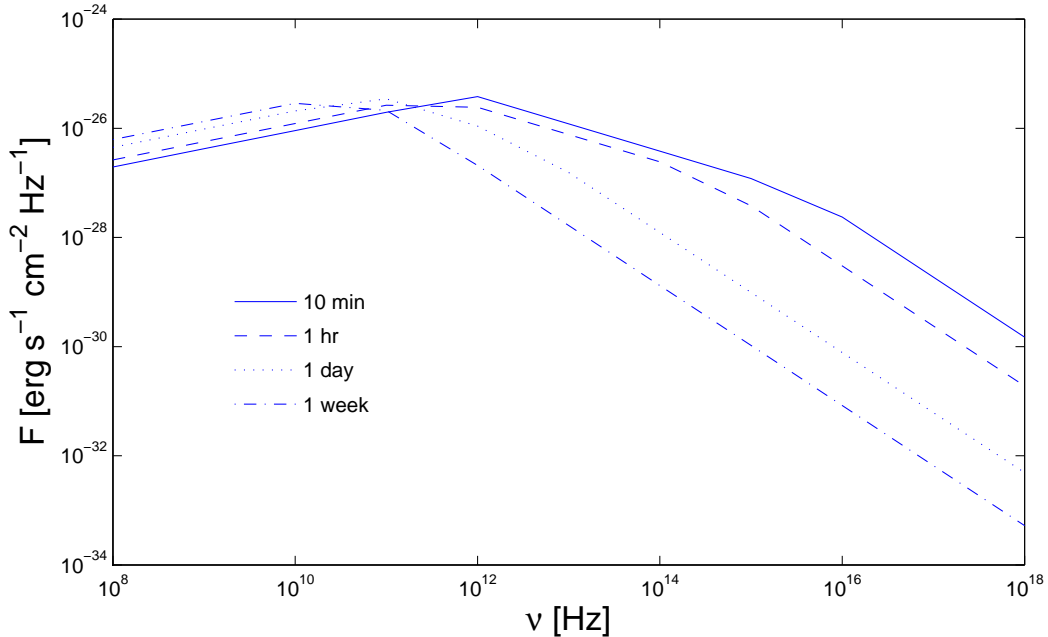


Figure 8: Afterglow spectra of a GRB at $z = 20$ as seen in the observers frame under the assumption that synchrotron processes in the shock following the GRB are responsible for the afterglow.

10 Observations

10.1 What do we expect to see with JWST?

We will now focus on a particular part of the spectrum we have just derived: the JWST window. We will compare the sensitivities of the filters on the NIRcam of JWST, as can be found on their website, and compare these with the afterglow spectra in the JWST window. This comparison is plotted for GRBs at $z = 10, 20, 30$ in figure 9. As one can see, the 10σ sensitivities of all the filters are sufficient to detect the afterglow spectra from the different redshifts, varying from 15σ for $z = 30$ to 60σ for $z = 10$, for the filter with the highest sensitivity. This is a significant result that tells us that it is in principle possible to detect the afterglow of a very high-redshift GRB.

10.2 Number of GRB in a random field

Now that we know that JWST does in principle enable us to detect a high-redshift GRB we would like to say something about the probability of detecting such an afterglow when we point the NIRcam at a random field at the sky. The field of the NIRcam is $2.6' \times 2.6'$. If we consider for example high-redshift GRBs from $z = 10$ to $z = 30$, we know from section 8.2 the number of halos within a mass bin dM around a halo of mass M .

As we can see there will be a lot of $10^6 M_\odot$ halos in our field, but will these halos produce a lot of GRBs? What we have not taken into account by now is that the amount of energy that is released during a PISN can be on the order of the gravitational binding energy of the

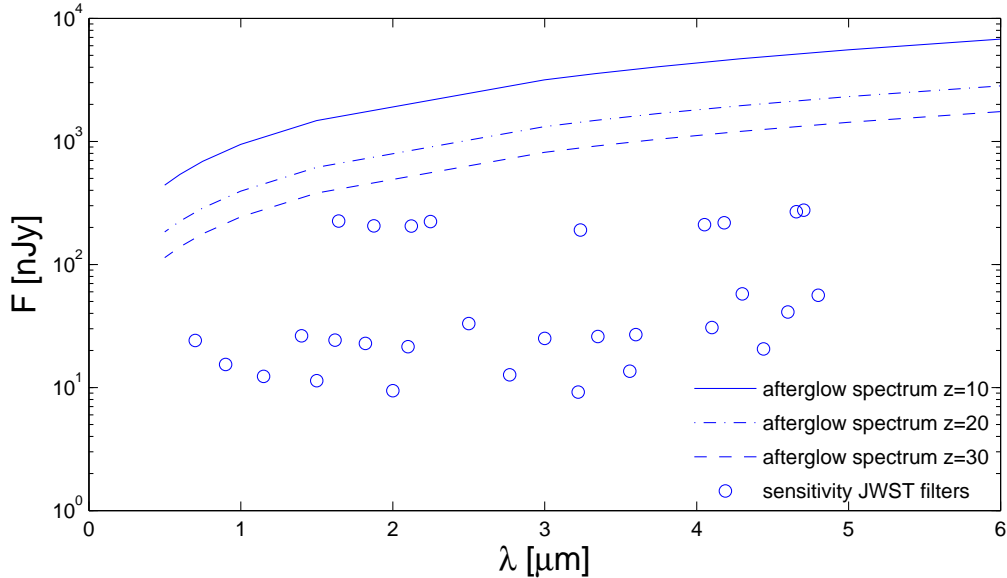


Figure 9: Afterglow spectra of a GRB after one week in JWST window at redshifts $z = 10$, $z = 20$ and $z = 30$. The circles show the 10σ sensitivities of the filters on the NIRcam after an integration of 10000 seconds.

halo. The binding energy of a $10^6 M_\odot$ halo is for example $\sim 10^{51}$ ergs whereas for a $10^7 M_\odot$ halo this is $\sim 10^{53}$ ergs. Therefore in a halo of $10^6 M_\odot$ one supernova like event that releases 10^{52} ergs of mechanical energy, is enough to blow away the complete halo whereas in a halo of $10^7 M_\odot$ you need only ~ 10 of these events to destroy the halo. In this case further star formation is of course halted so that the halo will also not be able to produce a GRB anymore. Since $\eta_{GRB} \ll 1$, we do not expect GRBs to occur in these halos. The binding energy of a $10^8 M_\odot$ halo is however significantly more than the 10^{52} ergs so that these halos will probably survive the supernova like events within them. We make the assumption here that halos with a mass higher than $3 \cdot 10^7 M_\odot$ will survive a supernova whereas lower mass halos will not. The total number of GRBs that we expect in our random field is therefore determined by halos with a mass higher than the cutoff mass of $3 \cdot 10^7 M_\odot$.

As a final thing we would like to derive an estimate for the number of GRB that we expect in our random field. For this, we will combine section 7 that provides us with the number of GRB that take place in a particular halo with section 8 that tells us how many of these halos we expect in our field.

Since we are interested in the halos between $z = 10$ and $z = 30$, we can use the prescriptions from figure 7 to derive the expected number of halos in our field. The values that are presented there are already integrated over time so that the power-law fit that was used to approximate the number of halos is only a function of halo mass. According to this fit, that was used to facilitate this derivation, in a field of $1' \times 1'$ the number of halos in a mass bin dM around halos with mass M is given by $\#_{halos}/1' \times 1' = 1.34 \cdot 10^{15} M_{halo}^{-2.08}$.

For the total number of GRBs N_{GRB} that occur in a particular halo we use the values presented in figure 5 for $z = 20$, fitted by $N_{GRB} = 4.1 \cdot 10^{-11} M_{halo}^{1.26}$. This total number does

not change drastically with redshift so that we take this as a constant from $z = 10$ to $z = 30$. As was explained previously the lower limit of the halos that we will take into account is $3 \cdot 10^7 M_\odot$. For the upper limit we will take $10^{11} M_\odot$. Combining all of these gives the following approximation to the total number of GRBs N_{field} in our random field with the NIRcam on JWST:

$$N_{field} \sim \theta_{JWST}^2 \int \#_{halos}(M_{halo}) \cdot N_{GRB}(M_{halo}) dM \sim 1.5 \cdot 10^8. \quad (55)$$

At first this might seem an amazingly large number, but we have to realize that we would only expect to observe such an amount of GRBs in our field if we make the rather naive assumption that all the halos in our field have at the particular time of observation just started to form stars out of zero-metallicity gas. A much more realistic assumption would for example be that the probability that a random halo has just started to form stars out of zero-metallicity gas is equally distributed over time between $z = 10$ and $z = 30$. Notice that from equation (4) we have a time span of $\sim 4 \cdot 10^8 \text{ yr}$ between $z = 10$ and $z = 30$, so that the latter probability would be $\sim \frac{1}{4 \cdot 10^8} \text{ yr}^{-1}$. In this case we would have to observe our random field for $\sim 3 \text{ yr}$ in order to detect one GRB! Therefore we conclude that it seems to be rather unlikely that we find the afterglow of a GRB when we point our telescope at a random field on the sky at a particular moment in time. In any case, follow-up of a GRB detected with GRBs detectors like the one on BeppoSax is fine of course.

11 Discussion and conclusion

Within the context of the collapsar model and the existing theories about population III star formation in a Λ CDM cosmology we have derived that the existence of very high redshift GRBs is very likely. Moreover, we have derived that it is in principle possible to detect the afterglow of such a high redshift GRB with JWST. The probability of detecting such an afterglow when we point JWST at a random field on the sky is however rather small. Therefore the detections of afterglows will for the time being remain dependent on satellites like BeppoSax that can monitor almost the entire sky for γ -flashes. Once such a flash has been detected, other telescopes like JWST can be guided to this position and try to detect an afterglow and possibly the spectrum of the afterglow.

Now that we finished the model it is time to look back and ask ourselves the question what it really tells us. For this, we should discuss the uncertainties in our model. The uncertainties in the model are mainly introduced by the assumptions we make and the uncertainties that are already present in values we take from other models. We will first take a closer look on the question whether the assumptions we made can be justified.

We started with a model of the star formation rate. In this, we assumed that the total star formation rate per unit area for population III stars is like in normal star formation given by the Schmidt-law. This Schmidt-law is more or less what you would expect when you divide the density by the freefall time. Since the physical meaning of these two quantities on which we expect the total star formation rate to depend does not change with time, it seems to be a reasonable assumption that the Schmidt-law is valid for star formation at high redshift. Like we did in our model, one should in this case of course use a value of the surface density that is characteristic for a population III environment. A second assumption that we made is that dark matter halos and the baryonic gas inside these halos undergo a spherical collapse. Although this is not completely true, in the high redshift universe that we are interested in,

this turns out to be a good approximation. The same holds for the assumption that stars form out of a spherical gas cloud.

In the normalization of the IMF for population III stars we assumed in the mass range of $100 - 500 M_{\odot}$ a flat IMF. This is a rather crude assumption, but the absence of observations make that we have to base our model on the data that follows from other models. The IMF of the first stars will however remain uncertain as long as observations do not become available. This lack of observations does also make the assumed fraction η_{GRB} of these stars that form a GRB, a highly uncertain value.

The way in which a halo is enriched with metals is also based on a model. This is again because there are no observations available of PISN and certainly not of their nucleosynthesis. It is however difficult to say something about the reliability of the data that we use from other models. All of these models make their own assumptions introducing resulting uncertainties.

The use of the Press-Schechter formalism as an indication of the abundance of dark matter halos hides a lot of information we would like to have. The formalism does only tell us the abundance of halos whereas we would also like to know for example when such a halo formed, when it started to form stars and what its starting metallicity is. The latter is related to the fact that the Press-Schechter formalism does only take into account gravity. In the context of the hierarchical clustering scenario smaller galaxies merge and form larger galaxies. When these smaller building blocks already had some episode of star formation this will give rise to a halo that is pre-enriched with metals. Pre-enrichment of the primordial gas can also be caused by the smallest halos that had some star formation before they were destroyed by the supernova-like events within them. As we have seen, above a metallicity of $10^{-2}Z_{\odot}$ we do not expect GRBs anymore. Our model does not take this into account.

Finally we assumed for the afterglow spectrum of the GRB a synchrotron spectrum as observed in normal shock waves. Since we think that the afterglow of a GRB is caused by such a shock wave, this seems to be a reasonable assumption.

Although we realize that each of the assumptions we make introduce some uncertainty, it is hard to say something quantitatively about the total uncertainty. Therefore it is at this point better to restate what conclusions we can draw from our model, despite the uncertainties that it contains. That is, our research tells us that within today's theoretical framework population III stars are a likely progenitor for GRBs and the model we developed showed that we should be able to use JWST to observe the afterglow of a such a GRB. Moreover our model showed that finding GRB afterglows will in the near future remain dependent on follow-up observations of GRBs observed by specific all-sky monitoring detectors.

References

- [1] T. Abel, G.L. Bryan & M.L. Norman. 2002. *The formation of the first star in the universe*. Science 295:93.
- [2] V. Bromm, P.S. Coppi & R.B. Larson. 2002. *The formation of the first stars I. The primordial star-forming cloud*. ApJ 564:23.
- [3] V. Bromm & R.B. Larson. 2004. *The first stars*. ARA&A 42:79.
- [4] V. Bromm & A. Loeb. 2007. *GRB cosmology*. arXiv:0706.2445v2.

- [5] B. Ciardi & A. Loeb. 2000. *Expected number and flux distribution of gamma-ray burst afterglows with high redshifts*. ApJ 540:687.
- [6] M.B. Davies, A.J. Levan, J. Larsson, A.R. King & A.S. Fruchter. 2007. *Progenitors of long gamma-ray bursts*. AIP Conference Proceedings 906:69.
- [7] L. Gao, N. Yoshida, T. Abel, C.S. Frenk, A. Jenkins & V. Springel. 2007. *The first generation of stars in the Λ cold dark matter cosmology*. MNRAS 378:449.
- [8] A. Heger and S. E. Woosley. 2002. *The nucleosynthetic signature of population III*. ApJ 567:532.
- [9] D.W. Hogg. 2000. *Distance measures in cosmology*. arXiv:astro-ph/9905116v4.
- [10] S. Inoue, K. Omukai & B. Ciardi. 2007. *The radio to infrared emission of very high redshift gamma-ray burst: probing early star formation through molecular and atomic absorption lines*. MNRAS 380:1715.
- [11] R. C. Kennicutt. 1998. *The global Schmidt law in star-forming galaxies*. ApJ 498:541.
- [12] N. Langer & C.A. Norman. 2006. *On the collapsar model of long gamma-ray bursts: constraints from cosmic metallicity evolution*. ApJ 638:L63.
- [13] C. A. Norman & M. Spaans. 1997. *Molecules at high redshift: the evolution of the cool phase of protogalactic disks*. ApJ 480:145.
- [14] K. Omukai & R. Nishi. 1998. *Formation of primordial protostars*. ApJ 508:141.
- [15] K. Omukai, T. Tsuribe, R. Schneider & A. Ferrara. 2005. *Thermal and fragmentation properties of star-forming clouds in low-metallicity environments*. ApJ 626:627.
- [16] J.A. Peacock. 1999. *Cosmological physics*. Textbook.
- [17] T. Piran. 1998. *Gamma-ray bursts and the fireball model*. arXiv:9810256v1.
- [18] W.H. Press & P. Schechter. 1974. *Formation of galaxies and clusters of galaxies by self-similar gravitational condensation*. ApJ 187:425
- [19] B.S. Ryden. 2002. *Introduction to cosmology*. Textbook.
- [20] M. Tegmark, J. Silk, M.J. Rees, A. Blanchard, T. Abel & F. Palla. 1997. *How small were the first cosmological objects?*. ApJ 474:1.
- [21] A.G.G.M. Tielens. 2005. *The physics and chemistry of the interstellar medium*. Textbook.
- [22] S. E. Woosley. 1993. *Gamma-ray bursts from stellar mass accretion disks around black holes*. ApJ 405:273.
- [23] R. Willingale, P.T. O'Brien, M.R. Goad, J.P. Osborne, K.L. Page & N.R. Tanvir. 2007. *A universal GRB photon energy-peak luminosity relation*. arXiv:0710.3727v1.
- [24] S.C. Yoon & N. Langer. 2005. *Evolution of rapidly rotating metal-poor stars towards gamma-ray bursts*. A&A 443:643.

- [25] S.C. Yoon, N. Langer & C. Norman. 2006. *Single star progenitors of long gamma-ray bursts I. Model grids and redshift dependent GRB rate.* A&A 460:199.
- [26] N. Yoshida, T. Abel, L. Hernquist & N. Sugiyama. 2003. *Simulations of early structure formation: primordial gas clouds.* ApJ 592:645.
- [27] N. Yoshida, K. Omukai, L. Hernquist & T. Abel. 2006. *Formation of primordial stars in a Λ CDM universe.* ApJ 652:6.
- [28] M. Zeilik & S.A. Gregory. 1998. *Introductory astronomy & astrophysics.* Textbook.